Table 2
Clinical Characteristics of 351 Patients Who Underwent HSCT

	BSI (n = 39)	No BSI (n = 312)	P
Sex, male/female, n	21/18	172/140	1.000
Age, yr, median	11	11	.568
Previous treatment, n (%)			
ATG	33 (85)	177 (57)	**.001**
CsA	34 (87)	210 (67)	**.010**
Both ATG and CsA	33 (85)	171 (55)	**<.001**
Bacterial/fungal infection at HSCT, n (%)	3 (8)	18 (6)	.716
First HSCT, n (%)	37 (95)	286 (92)	.754
Stem cell source, n (%)			.959
BM	35 (90)	280 (90)	
PB	1 (3)	11 (4)	
BM + PB	0 (0)	1 (0)	
CB	3 (8)	20 (6)	
Donor, n (%)			**.044**
Syngeneic	0 (0)	1 (0)	
Related	12 (31)	161 (52)	
Unrelated	27 (69)	150 (48)	
Receipt of ≥20 transfusions before HSCT, n (%)			
RBCs	20 (51)	84 (27)	**.003**
Platelets	21 (54)	102 (33)	**.012**
ABO type match, n (%)			**.014**
Match	16 (41)	172 (55)	
Major mismatch	14 (36)	47 (15)	
Minor mismatch	6 (15)	54 (17)	
Major plus minor mismatch	3 (8)	39 (13)	
HLA compatibility (low-resolution typing), n (%)			.846
Matched	30 (77)	231 (74)	
Mismatched	9 (23)	81 (26)	
Conditioning regimen, n (%)			
ATG	30 (77)	210 (67)	.275
Fludarabine	27 (69)	217 (70)	1.000
Cyclophosphamide	36 (92)	281 (90)	1.000
Irradiation	33 (85)	231 (74)	.173
GVHD prophylaxis, n (%)			
Steroid	0 (0)	17 (5)	.235
CsA	11 (28)	149 (48)	**.040**
Tacrolimus	28 (72)	163 (52)	**.026**
Methotrexate	37 (95)	282 (90)	.555
Acute GVHD grade II-IV, n (%)	5 (13)	55 (18)	.651
Graft failure, n (%)	5 (13)	16 (5)	.070
Time from diagnosis to HSCT, d, median	447	305.5	**.020**
Time from diagnosis to HSCT >300 d, n (%)	30 (77)	157 (50)	**.002**
Severity at diagnosis, n (%)			.641
Very severe	7 (18)	77 (25)	
Severe	16 (41)	121 (39)	
Nonsevere	16 (41)	114 (37)	
Severity at HSCT, n (%)			.426
Very severe	17 (44)	105 (34)	
Severe	15 (38)	151 (48)	
Nonsevere	7 (18)	56 (18)	

BM indicates bone marrow; PB, peripheral blood; CB, cord blood.
*Irradiation included total body irradiation, thoracoabdominal irradiation, and total lymphoid irradiation.

11.63% versus 95.84% ± 1.66%; $P = .0379$). Univariate analysis of variables associated with BSI identified age ≥14 years at HSCT as the sole risk factor (Table 4).

Assessment of BSI in 165 Patients Who Underwent First HSCT from an Unrelated Donor

BSI occurred in 26 of 165 patients with AA who underwent a first HSCT from an unrelated donor (15.8%). The 5-year overall survival rate was lower in patients with complicated BSI compared with those without BSI (55.75% ± 10.14% versus 90.77% ± 2.25%; $P < .0001$). In univariate analysis, variables associated with BSI included a history of immunosuppressive therapy with ATG, frequent blood transfusion before transplantation, graft failure, and major or major plus minor ABO type mismatch (Table 4).

Table 3
Multivariate Analysis of 351 Patients with AA

	Hazard Ratio	P	95% Confidence Interval
Interval from diagnosis to HSCT >300 d	2.430	**.041**	1.036-5.702
≥20 RBC or platelet transfusions before HSCT	1.843	.109	0.873-3.891
Major or major plus minor ABO type mismatch	1.595	.199	0.783-3.250
Unrelated donor	1.233	.673	0.466-3.262
Use of tacrolimus	1.167	.755	0.442-3082
Previous treatment with ATG or CsA	1.115	.839	0.392-3.170

DISCUSSION

In the literature, the incidence of BSI after the early phase of HSCT in children has ranged from 25% to 30% [4-8]. In our previous study, the incidence of BSI after HSCT (including patients with malignant and nonmalignant diseases) was 8.7% [6]. In the study of Sarashina et al. [6], nonmalignant disease, especially AA and Wiskott-Aldrich syndrome, were identified as risk factors for BSI after HSCT (17.2%).

The present study is the first to analyze BSI after HSCT in pediatric patients with AA. Our data show a lower incidence of BSI in these patients (11.1%) compared with our previous study, but a higher incidence than that seen in patients with other diseases in that study. In our previous study, BSI was not associated with survival, and the survival rate was nearly identical in patients with BSI and those without BSI; however, in the present study, the survival rate was lower in patients with BSI. Patients with malignant diseases were included in the previous study, whereas only patients with AA were analyzed in the present study. In patients with malignant disease, the relapse rate of the original disease was lower in patients with BSI; this difference might account for the discrepant results between the previous and present studies.

In the present study, univariate analysis identified a history of immunosuppressive therapy with ATG, receipt of a transplant from an unrelated donor, frequent blood transfusions before HSCT, major or major plus minor ABO type mismatch, GVHD prophylaxis with tacrolimus but without CsA, and extended interval from diagnosis to HSCT as risk factors for BSI. Poutsiaka et al. [9] previously reported an association between BSI after HSCT and acute GVHD; however, our data do not corroborate this finding. Interestingly, the risk factors for BSI identified in the present study are associated with one another. Generally, patients without a related HLA-matched donor are treated with immunosuppressive therapy. If this therapy is not effective, then HSCT with an unrelated donor is performed. These patients often receive numerous blood transfusions and have a extended interval between diagnosis and transplantation. Furthermore, tacrolimus (rather than CsA) may be selected for GVHD prophylaxis. Among these factors, an extended interval between diagnosis and HSCT was the sole statistically significant risk factor for BSI identified by multivariate analysis.

Regarding numerous blood transfusions before HSCT, some recent studies have investigated the relationship

Table 4
Clinical characteristics of 158 patients who underwent HSCT from related donor as first HSCT and 165 patients who underwent HSCT from unrelated donor as first HSCT

	Related Donor (n = 158)			Unrelated Donor (n = 165)		
	BSI (n = 11)	No BSI (n = 147)	*P*	BSI (n = 26)	No BSI (n = 139)	*P*
Sex, male/female, n	6/5	84/63	1.000	10/16	77/62	.136
Age, yr, median	15	11	**.050**	11	11	.675
Age ≥14 yr, n (%)	8 (73)	45 (31)	**.007**			
Previous treatment, n (%)						
ATG	5 (45)	49 (33)	.512	25 (96)	110 (79)	**.050**
CsA	6 (56)	68 (46)	.756	25 (96)	124 (89)	.472
Both ATG and CsA	5 (45)	48 (33)	.509	25 (96)	107 (77)	.030
Bacterial/fungal infection at HSCT, n (%)	2 (18)	10 (7)	.198	1 (4)	7 (5)	1.000
Stem cell source, n (%)			.863			.734
BM	10 (91)	139 (95)		23 (88)	125 (90)	
PB	1 (9)	6 (4)		0 (0)	0 (0)	
BM + PB	0 (0)	1 (1)		0 (0)	0 (0)	
CB	0 (0)	1 (1)		3 (12)	14 (10)	
Donor, n (%)			1.000			
Syngeneic	0 (0)	1 (1)		-	-	
Related	11 (100)	146 (99)		-	-	
Receipt of ≥20 transfusions before HSCT, n (%)						
RBCs	2 (18)	10 (7)	.198	17 (65)	57 (41)	**.031**
Platelets	3 (27)	26 (18)	.425	17 (65)	58 (42)	**.032**
ABO type match, n (%)			.718			**.024**
Match	7 (64)	97 (66)		8 (31)	62 (45)	
Major mismatch	2 (18)	18 (12)		12 (46)	26 (19)	
Minor mismatch	2 (18)	20 (14)		3 (12)	29 (21)	
Major and minor mismatch	0 (0)	12 (8)		3 (12)	22 (16)	
HLA compatibility (low-resolution typing), n (%)			1.000			.248
Matched	9 (82)	122 (83)		21 (78)	95 (68)	
Mismatched	2 (18)	25 (17)		5 (22)	44 (32)	
Conditioning regimen, n (%)						
ATG	7 (64)	91 (62)	1.000	22 (81)	108 (78)	.602
Fludarabine	5 (45)	87 (59)	.528	20 (77)	109 (78)	.333
Cyclosphosphamide	10 (91)	138 (94)	.525	24 (92)	130(94)	.685
Irradiation	6 (56)	85 (58)	1.000	25 (96)	128 (92)	.693
GVHD prophylaxis, n (%)						
Steroid	0 (0)	4 (3)	1.000	0 (0)	10 (7)	.365
CsA	10 (91)	119 (81)	.690	1 (4)	20 (14)	.203
Tacrolimus	1 (9)	28 (19)	.690	25 (96)	119 (86)	.203
Methotrexate	10 (91)	131 (89)	1.000	25 (96)	132 (95)	1.000
Acute GVHD grade II-IV, n (%)	0 (0)	13 (9)	.601	5 (19)	37 (27)	.624
Graft failure, n (%)	0 (0)	5 (3)	1.000	5 (19)	7 (5)	**.024**
Mean time from diagnosis to HSCT, d	91	80	.426	474.5	455	.183
Severity at diagnosis, n (%)			.735			.664
Very severe	2 (18)	41 (28)		5 (19)	35 (25)	
Severe	5 (45)	65 (44)		10 (38)	42 (30)	
Nonsevere	4 (36)	41 (28)		11 (42)	62 (45)	
Severity at HSCT, n (%)			.490			.094
Very severe	5 (45)	59 (40)		12 (46)	35 (25)	
Severe	3 (27)	64 (44)		10 (38)	75 (54)	
Nonsevere	3 (27)	24 (16)		4 (15)	29 (21)	

*Irradiation included total body irradiation, thoracoabdominal irradiation, and total lymphoid irradiation.

between pretransplantation hyperferritinemia and post-transplantation outcomes [10,11]. In many of these reports, hyperferritinemia was associated with adverse outcomes after allogeneic HSCT. Moreover, iron overload is associated with proliferation of bacteria and fungus [12]. These observations suggest that iron chelating agents should be administered before HSCT in patients who have received frequent blood transfusions.

We analyzed BSI after HSCT in patients undergoing first transplantation from related and unrelated donors to clarify the risk factors for BSI. In both groups, survival rates were significantly lower in patients with BSI than in those without BSI. Surprisingly, the survival rate of patients undergoing HSCT from an unrelated donor without BSI exceeded 90%, not significantly different from that seen in patients undergoing HSCT from a related donor. This finding suggests that prevention of BSI is important to improving outcomes after HSCT. In patients who underwent HSCT from a related donor, age ≥14 years at transplantation was identified as a risk factor for BSI, although the incidence of BSI was evidently lower than that in patients undergoing HSCT from an unrelated donor. Older patients tend to have more severe oral mucositis. Furthermore, we previously identified age >10 years as a risk factor for fungal infection in patients with hematologic malignancies [13]. In contrast, in patients who underwent HSCT from an unrelated donor, variables associated with BSI included a history of immunosuppressive therapy with ATG, frequent transfusions before transplantation, graft failure, and major or major plus minor ABO type mismatch.

The impact of ABO incompatibility on clinical outcomes remains controversial [14,15]. ABO incompatibility in

allogeneic HSCT is associated with an increased risk of delayed erythroid reconstitution, pure RBC aplasia, and acute and delayed hemolysis; however, ABO incompatibility has not been identified as a risk factor for BSI. The ABO blood group antigens consist of oligosaccharide glycoproteins and are expressed in erythrocytes as well as in neutrophils, platelets, and vascular endothelial and epithelial cells. The ABO antigens could be immunologic targets for ABO-incompatible donor or recipient lymphocytes, thereby affecting GVHD and engraftment [16]. These phenomena may contribute to the development of BSI.

In conclusion, because the 5-year overall survival rate without BSI exceeded 90%, even in patients who underwent HSCT from an unrelated donor, controlling BSI is very important for a successful outcome of HSCT in patients with pediatric AA.

ACKNOWLEDGMENTS

Conflict of Interest Statement: There are no conflicts of interest to report.

Financial disclosure: The authors have no support or funding to report.

REFERENCES

1. Kikuchi A, Yabe H, Kato K, et al. Long-term outcome of childhood aplastic anemia patients who underwent allogeneic hematopoietic SCT from an HLA-matched sibling donor in Japan. *Bone Marrow Transplant.* 2013;48:657-660.
2. Kojima S, Hibi S, Kosaka Y, et al. Immunosuppressive therapy using antithymocyte globulin, cyclosporine, and danazol with or without human granulocyte colony-stimulating factor in children with acquired aplastic anemia. *Blood.* 2000;96:2049-2054.
3. Meyers G, Maziarz RT. Is it time for a change? The case for early application of unrelated allo-SCT for severe aplastic anemia. *Bone Marrow Transplant.* 2010;45:1479-1488.
4. Romano V, Castagnola E, Dallorso S, et al. Bloodstream infections can develop late (after day 100) and/or in the absence of neutropenia in children receiving allogeneic bone marrow transplantation. *Bone Marrow Transplant.* 1999;23:271-275.
5. Engelhard D. Bacterial and fungal infections in children undergoing bone marrow transplantation. *Bone Marrow Transplant.* 1998;21(Suppl 2):S78-S80.
6. Sarashina T, Yoshida M, Iguchi A, et al. Risk factor analysis of bloodstream infection in pediatric patients after hematopoietic stem cell transplantation. *J Pediatr Hematol Oncol.* 2013;35: 76-80.
7. Camitta BM, Thomas ED, Nathan DG, et al. A prospective study of androgens and bone marrow transplantation for treatment of severe aplastic anemia. *Blood.* 1979;53:504-514.
8. Kersun LS, Propert KJ, Lautenbach E, et al. Early bacteremia in pediatric hematopoietic stem cell transplant patients on oral antibiotic prophylaxis. *Pediatr Blood Cancer.* 2005;45:162-169.
9. Poutsiaka DD, Munson D, Price LL, et al. Bloodstream infection (BSI) and acute GVHD after hematopoietic SCT (HSCT) are associated. *Bone Marrow Transplant.* 2011;46:300-307.
10. Altès A, Remacha AF, Sureda A, et al. Iron overload might increase transplant-related mortality in haematopoietic stem cell transplantation. *Bone Marrow Transplant.* 2002;29:987-989.
11. Armand P. Hyperferritinemia in stem cell transplantation. *Biol Blood Marrow Transplant.* 2013;19:336-337.
12. Miceli MH, Dong L, Grazziutti ML, et al. Iron overload is a major risk factor for severe infection after autologous stem cell transplantation: a study of 367 myeloma patients. *Bone Marrow Transplant.* 2006;37: 857-864.
13. Kobayashi R, Kaneda M, Sato T, et al. The clinical feature of invasive fungal infection in pediatric patients with hematologic and malignant diseases: a 10-year analysis at a single institution at Japan. *J Pediatr Hematol Oncol.* 2008;30:886-890.
14. Booth GS, Gehrie EA, Bolan CD, Savani BN. Clinical guide to ABO-incompatible allogeneic stem cell transplantation. *Biol Blood Marrow Transplant.* 2013;19:1152-1158.
15. Rowley SD, Donato ML, Bhattacharyya P. Red blood cell–incompatible allogeneic hematopoietic progenitor cell transplantation. *Bone Marrow Transplant.* 2011;46:1167-1185.
16. Konuma T, Kato S, Ooi J, et al. Effect of ABO blood group incompatibility on the outcome of single-unit cord blood transplantation after myeloablative conditioning. *Biol Blood Marrow Transplant.* 2014;20: 577-581.

SCIENTIFIC REPORTS

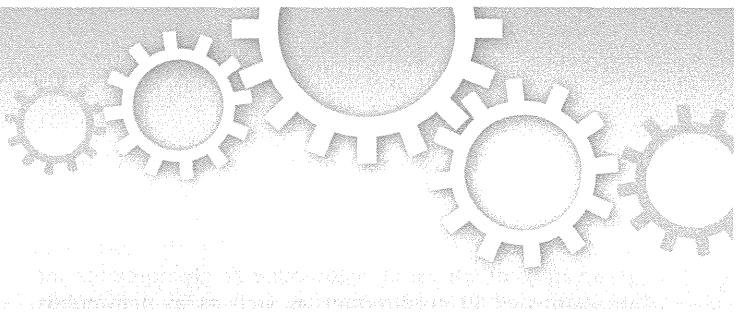

OPEN

SUBJECT AREAS:
CYTOGENETICS
HERPES VIRUS

Received
13 November 2013

Accepted
17 March 2014

Published
2 April 2014

Correspondence and requests for materials should be addressed to H.K. (kura@fujita-hu.ac.jp)

Dual roles for the telomeric repeats in chromosomally integrated human herpesvirus-6

Tamae Ohye[1], Hidehito Inagaki[1], Masaru Ihira[2,3], Yuki Higashimoto[2,4], Koji Kato[5], Junko Oikawa[6], Hiroshi Yagasaki[7], Takahiro Niizuma[8,9], Yoshiyuki Takahashi[10], Seiji Kojima[10], Tetsushi Yoshikawa[2] & Hiroki Kurahashi[1]

[1]Division of Molecular Genetics, Institute for Comprehensive Medical Science, Fujita Health University, Toyoake, Aichi 470-1192, Japan, [2]Department of Pediatrics, Fujita Health University School of Medicine, Toyoake, Aichi 470-1192, Japan, [3]Faculty of Clinical Engineering, Fujita Health University School of Health Sciences, Toyoake, Aichi 470-1192, Japan, [4]Department of Laboratory Medicine, Fujita Health University Hospital, Toyoake, Aichi 470-1192, Japan, [5]Department of Hematology and Oncology, Children's Medical Center, Japanese Red Cross Nagoya First Hospital, Nagoya, Aichi 453-8511, Japan, [6]Department of Pediatrics, Chiba University School of Medicine, Chiba, Chiba 260-8670, Japan, [7]Department of Pediatrics, School of Medicine, Nihon University, Itabashi-ku, Tokyo 173-8610, Japan, [8]Department of Pediatrics, Koshigaya Municipal Hospital, Koshigaya, Saitama 343-8577, Japan, [9]Department of Pediatrics, Tokyo Rinkai Hospital, Edogawa-ku, Tokyo 134-0086, Japan, [10]Department of Pediatrics, Nagoya University Graduate School of Medicine, Nagoya, Aichi 466-8550, Japan.

Approximately 1 percent of healthy individuals carry human herpesvirus-6 within a host chromosome. This is referred to as chromosomally integrated herpesvirus-6 (CIHHV-6). In this study, we investigated the chromosomal integration site in six individuals harboring CIHHV-6B. Using FISH, we found that HHV-6B signals are consistently located at the telomeric region. The proximal endpoints of the integrated virus were mapped at one of two telomere-repeat-like sequences (TRSs) within the DR-R in all cases. In two cases, we isolated junction fragments between the viral TRS and human telomere repeats. The distal endpoints were mapped at the distal TRS in all cases. The size of the distal TRS was found to be ~5 kb which is sufficient to fulfill cellular telomeric functions. We conclude that the viral TRS in the DR regions fulfill dual functions for CIHHV-6: homology-mediated integration into the telomeric region of the chromosome and neo-telomere formation that is then stably transmitted.

Human herpesvirus 6 (HHV-6) is one of the best characterized family members of the nine human herpesviruses. HHV-6 is classified as two distinct species, designated HHV-6A and HHV-6B, with an overall nucleotide sequence identity of 90%[1–3]. It has been demonstrated that primary HHV-6B infection occurs in infancy and causes a common febrile exanthematous illness, exanthem subitum[4,5]. However, neither the clinical features of primary HHV-6A infection nor the diseases directly associated with it have been identified to date. Following primary infection, HHV-6 remains latent in monocytes/macrophages and persists in the salivary glands[6,7]. In transplant recipients, HHV-6B reactivation can cause several clinical conditions such as encephalitis, bone marrow suppression, and pneumonitis[8,9].

Accumulating evidence now indicates that a subset of normal healthy individuals carry the HHV-6 genome within their chromosomes, which is known as chromosomally integrated herpesvirus-6 (CIHHV-6)[10]. The virus genome in these cases is transmitted by Mendelian inheritance. The integrated virus itself does not appear to be pathogenic, but CIHHV-6 carriers are often identified as high-titer virus carriers during screenings for HHV-6 reactivation in immunocompromised hosts. The presence of CIHHV-6 is not a rare condition with a reported incidence in healthy individuals of 1% in Caucasians and 0.21% in Japanese populations[11–13].

Based on consistently detectable FISH signals at chromosome ends in all previously analyzed independent CIHHV-6 cases, it had been speculated that the HHV-6 viral genome is integrated into human telomeres through an unknown mechanism that is specific to HHV-6[14]. The HHV-6 genome comprises a linear double stranded DNA of 159 kb flanked by identical 8 kb direct repeats at the left and right ends (DR-L and DR-R). Each DR contains two human telomere repeat (TTAGGG)-like sequences (TRS) proximal to both ends of the DRs[15,16]. The function of these motifs is uncertain, but it is not unreasonable to hypothesize that they plays a role in protection of viral genome ends from host defense systems such as nucleases in a similar manner to the telomere protection

from DNA end repair systems in eukaryotes[17]. Recently, sequence analysis of the junction fragments of three individuals with CIHHV-6A revealed that the HHV-6 genome was directly joined with the human telomeric region via TTAGGG repeats in each case[18]. A homology-directed mechanism operated by host DNA damage repair response pathways such as homologous recombination is likely to mediate these rearrangements[19].

To further elucidate the mechanism of the viral integration into the human telomeres, we investigated the integration sites in six Japanese individuals harboring CIHHV-6B.

Results

Six cases that were suspected to CIHHV-6B by having genome-equivalent copy number of viral DNA in peripheral blood samples estimated by qPCR were analyzed[20]. Standard cytogenetic evaluations revealed no abnormalities in any of these subjects. FISH analysis with a HHV-6 genomic DNA probe detected virus-specific signals on the long arm of chromosome 22 in two cases (cases 18 and 19), on the long arm of chromosome 6 in one case (case 31), and on the short arm of chromosome X in the two cases (cases 28 and 63) (Fig. 1b–d). The mother of case 19 (case 20) was also analyzed and showed HHV-6 signals on the long arm of chromosome 22. Thus, a CIHHV-6B diagnosis was confirmed in all six study subjects. CIHHV-6B FISH signals were detectable on only one of the homologues in each case, suggesting that all six individuals were heterozygotes in terms of viral integration. HHV-6 signals were consistently detected at the end of the chromosomes, presumably at the telomeric regions, in all six cases.

To next determine the structure of the integrated viral genome in our subjects, we performed MLPA experiments which allowed us to determine copy number of the target sites of the viral genome relative to the chromosomal DNA in each case. The copy numbers for the UL regions were constant and similar to the chromosomal regions used as references (Fig. 2), suggesting that a single copy of the viral genome was integrated within the chromosomal DNA in our CIHHV-6 cases. Copy numbers for the DRs varied among the subjects; two-fold higher than those for the UL regions in cases 18, 19, and 20, three-fold higher in case 28, and at a similar level in case 31.

To map the breakpoints of the HHV-6 integration in more detail in our subjects, Southern analyses using several HHV-6 probes were performed. Since the two TRS regions in the DR-R are good candidates for viral integration breakpoints, DR probes located near to the TRS-2 site were used (Supplementary Fig. S1). These DR probes yielded two distinct bands of a similar intensity (Fig. 3a). One of the bands was detected at a similar position in all cases with a size that was expected for the DR-L, suggesting that the DR-L was intact. The sizes of second band were different in each case, although two cases that were found to carry the HHV-6B at the long arm of chromosome 22 showed a second band of similar size. This suggests that these fragments included the junction between the viral and human genome. According to the restriction map, the breakpoints were predicted to be located within the TRS-2. A similar band pattern in two cases with a 22q integration indicated a common founder for this integration event. The fact that two bands were detectable in these analyses suggests that the entire viral genome was inserted together with both the DR-L and DR-R. The fact that the intensities of the two detected bands were similar further supports the idea that only a single copy of entire HHV-6B genome had been inserted in each individual.

We next attempted to isolate the junction fragments and could fortunately rely on sequence information for the subtelomere-telomere junction in the Xp region. First, we performed PCR using a primer designed to amplify the subtelomeric region flanking the telomere repeats and a primer that recognized the UL region just outside of the DR-R. The amplification reactions appeared to yield no product, but subsequent Southern hybridization analysis detected

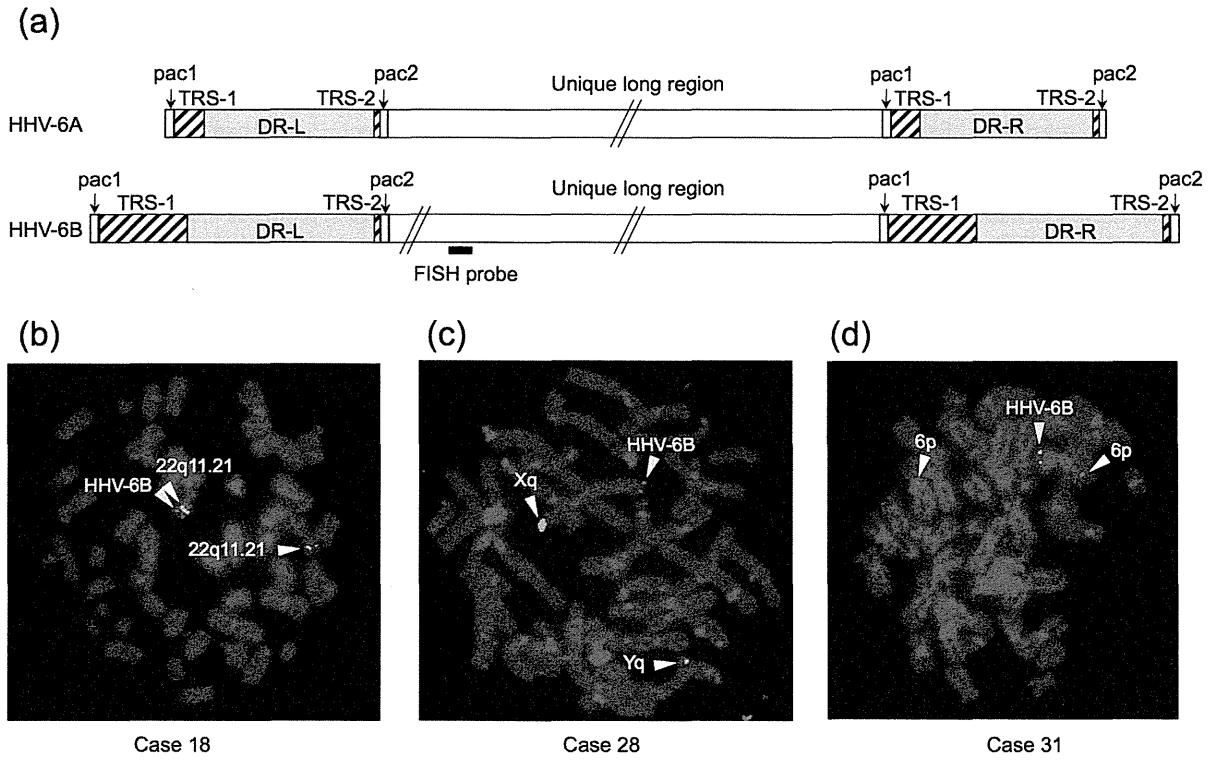

Figure 1 | Characterization of CIHHV-6B by FISH. (a) Schematic representation of the HHV-6 genomic structure. The 10 kb Pst I fragment used as s FISH probe is indicated. Gray boxes indicate DR sites and hatched boxes indicate TRS regions. (b) FISH analyses of metaphase chromosomes derived from the CIHHV-6B study subjects. A signal from the HHV-6B probe is detectable at the end of chromosome 22q (case 18), chromosome 6q (case 31) or chromosome Xp (case 28) (yellow arrowheads). The reference signals for chromosome 22q11.21, 6p and Xq are indicated by white arrowheads.

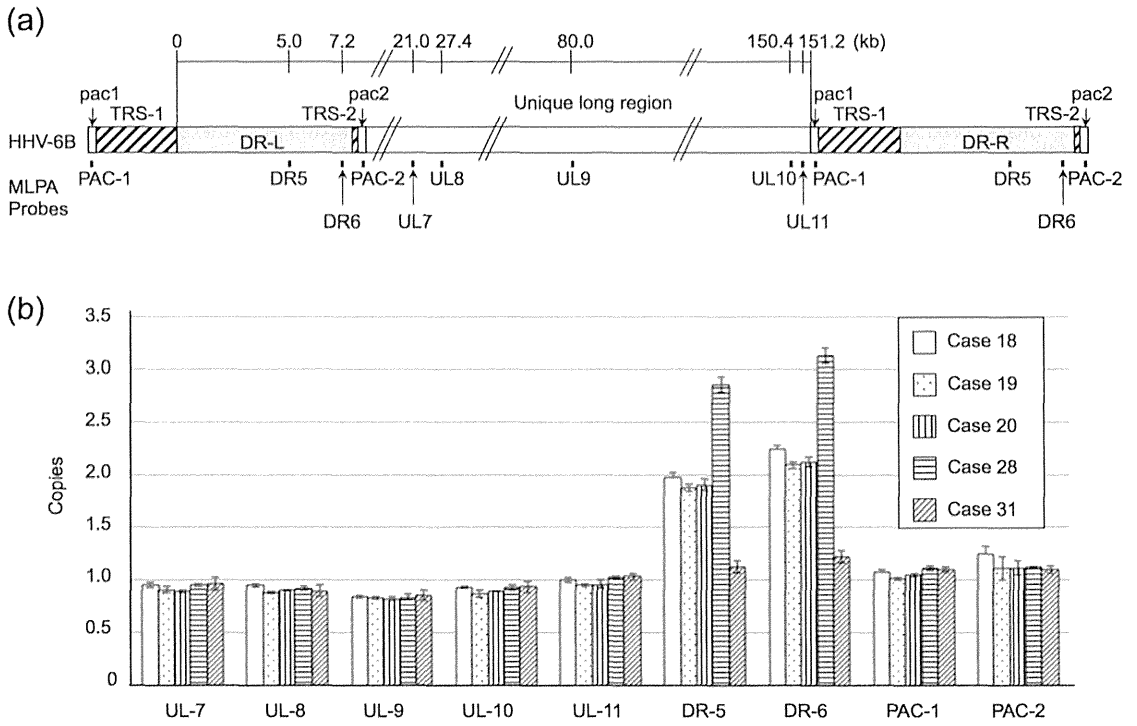

Figure 2 | Analyses of the CIHHV-6B genome structure by MLPA. (a) Schematic representation of the HHV-6B genome. The positions of the MLPA probes are indicated below the diagram. The scale bar indicates the distance from the starting point of DR-L. (b) Results of MLPA analyses. The vertical axis indicates the viral genome copy numbers relative to the single copy human genomic region. Data for cases 18, 19, 20, 28 and 31 are indicated from left to right.

a fragment exceeding 10 kb in length in case 28 with a HHV-6 integration at chromosome Xp (Fig. 3b). This indicated that the breakpoints of the virus were located within the DR-R. Unfortunately, less sequence information was available for the subtelomeric regions of chromosomes 6q and 22q. We attempted to perform junction PCR using a primer that bound to the most distal end of the reported subtelomeric sequence and a primer that recognized a region just outside of the DR-R, but no amplicon was obtained. We also tried inverse PCR but failed, because a short PCR product derived from short TTAGGG repeat present in the DR-L inhibited the amplification of real junction.

To further narrow down the positions of the HHV-6 breakpoints, multiple PCR primers were designed within the DR. Combined with a subtelomeric primer designed on the basis of sequence information for the Xp subtelomere-telomere junction (hg19, chrX: 60,427–60,445), all of the primers that recognized sites within the DR yielded PCR products of the expected size, which confirmed that the viral breakpoint is located within the TRS-2 (Fig. 3c). Sequencing of these amplicons revealed that the subtelomeric and viral DR-R regions were connected via 166 copies of the TTAGGG repeat, which is much shorter than the typical telomere repeat region in humans (9-15 kb; Fig. 3d) (GenBank accession number AB822541). These PCR experiments also yielded junction products in case 63 who had a HHV-6 integration at chromosome Xp. The sequence of this amplified fragment indicated that the integration sites are identical and the differences in the PCR product sizes was due to varying numbers of telomere repeats.

In one of our study subjects (case 31), the results of MLPA revealed only one copy of the DR, which was a similar level to the UL. Southern hybridization results for case 31 also produced a distinct pattern. A DR probe detected no bands corresponding to the DR-R, but constant bands only corresponding to the DR-L, suggesting that the TRS-2 had been deleted and that the HHV-6 breakpoint is located at a more distal region in this subject (Fig. 3a). Since TRS-1 is another candidate for the viral breakpoint, PCR for this region was performed using a DR primer flanking the TRS-1 site and a primer that was located just outside of the DR-R. No PCR product was obtained for case 31 although a TRS-1 amplicon was obtained in all other subjects, suggesting that the breakpoint in this one subject was located within the TRS-1 site in the DR-R (Supplementary Fig. S2a). Unexpectedly, the sizes of the TRS-1 PCR products from other cases were much larger (~5 kb) than that reported in the database (~300 bp), and also than TRS-2 (~500 bp). Although TRS-1 is referred to as heterogeneous $(TTAGGG)_n$ due to the reported presence of imperfect repeats, sequence analyses of our study subjects revealed a much longer stretch of perfect TTAGGG repeats than has been previously reported for the TRS-1 site, and greater also than those of TRS-2.

In case 28, MLPA results revealed a three-fold higher copy number for the DR compared with the UL region. Southern analyses further demonstrated the presence of additional DR copies in this subject, evidenced by three distinct bands (Fig. 3a). Sizes of the restriction fragments detected by DR probes suggested a proximal-DR-DR-UL-DR-distal structure within the genome of this individual (Supplementary Fig. S1, S3, and S4). To reveal the junction of the two distal DRs in this case, we performed PCR encompassing the TRS-2 – pac2 – pac1 – TRS-1 region. Only case 28 yielded a junction-specific PCR product that was also yielded from the subject including the replicating HHV-6B obtained from patients with exanthema subitum (Supplementary Fig. S5a). However, sequence analyses revealed that the junction between the two DRs in case 28 did not include pac1 or pac2, although the junction from the replicating HHV-6B carried the pac1 and pac2 regions.

To determine the structure of the other end of the HHV-6B genome, we mapped the endpoint of the viral genome within the DR-L. PCR amplification of the TRS-2 site in the DR-L was performed, and amplicons were obtained for all of our CIHHV-6B subjects. This suggested that the TRS-2 region in the DR-L had remained intact

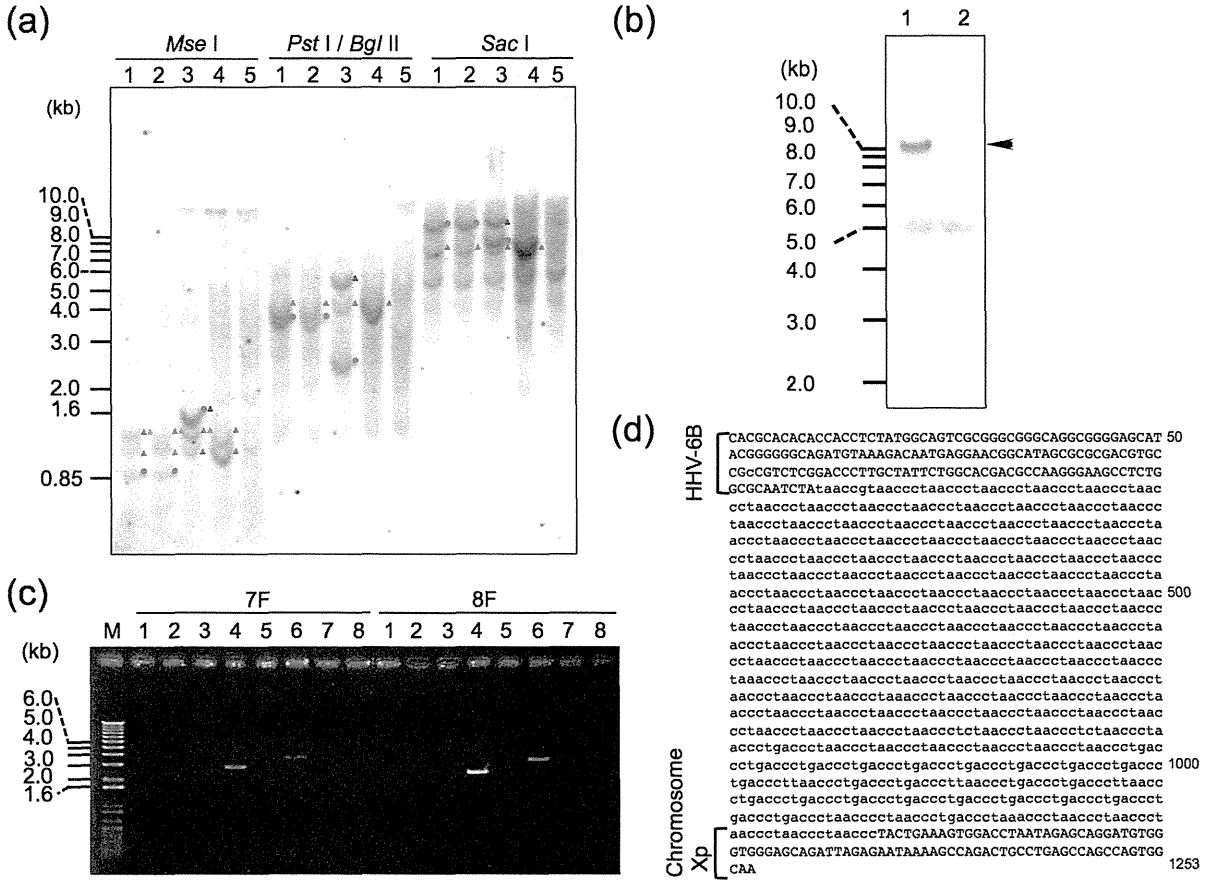

Figure 3 | Analyses of the junction between the human chromosome and viral genome. (a) Southern blot analyses of genomic DNA from the CIHHV-6B study subjects. The restriction enzymes used for these analyses are indicated above the panels; size markers are indicated on the left. Red dots indicate the rearranged bands derived from junction between human telomere and the HHV-6. Triangles indicate bands derived from the DR-L (green) and DR-R (orange), while blue triangles indicate the junction of the two DRs. Lane 1, case 18; lane 2, case 19; lane 3, case 28; lane 4, case 31; lane 5, non-CIHHV-6 control. (b) Southern blot analyses of PCR products. The arrowhead indicates a junction-specific PCR product. Lane 1, case 28; lane 2, non-CIHHV-6. Complete raw autoradiogram image can be seen in Supplementary Fig. S6. (c) PCR products that incorporate junction fragments. The primer sets were designed on the DR region (7F or 8F) and subtelomeric region on chromosomes X. Two CIHHV-6 cases yielded amplicons of different sizes. Lane M, size markers; lane 1, case 18; lane 2, case 19; lane 3, case 20; lane 4, case 28; lane 5, case 31; lane 6, case 63; lane 7, non-CIHHV-6 case; lane 8, water control. (d) Sequence of the junctions in case 28. The sequence shown covers the region from the DR-R of the viral genome to the human subtelomeric region. Lowercase letters denote telomere repeats.

in all cases (Supplementary Fig. S2b). We next performed PCR using one fixed primer for the site just outside of the DR-L and other primers for different sites within the DR. All of the primers within the DR successfully amplified specific products (Fig. 4). A telomere-repeat primer also yielded products appearing as a smear, the specificity of which was confirmed by Southern hybridization (Supplementary Fig. S5b). However, the use of a primer for the pac1 site did not yield any specific product. We also designed MLPA probes within the pac1 or pac2 region which produced a single copy signal which was similar to the UL region (Fig. 2), suggesting the absence of the pac1 site. These results demonstrated that the CIHHV-6B chromosome ends within the TRS-1.

The presence of the TRS-2 in the DR-L not only indicated an intact TRS-2, but also gave us the opportunity to analyze individual variations in the TTAGGG repeat numbers. As expected, the sizes of the PCR products varied among individuals (Supplementary Fig. S2b)[21]. Among three of our study subjects with an integration at 22q, two cases from the same family (cases 19 and 20) showed an amplified product of the same size. The other case with a viral integration at 22q (case 18) showed a PCR product of a similar size but subsequent sequence analysis revealed different numbers of telomere repeats (32 for cases 19 and 20 versus 29 for case 18). Two cases with a viral integration at Xp showed different numbers of repeats (27 for case 28 and 23 for case 63).

Discussion

In our present study, we analyzed the structure of the integrated HHV-6B genome in six carriers of this virus using the MLPA technique. Achieving accuracy in copy number measurements poses particular challenges when attempting to characterize a tandem repeat region. The MLPA method shows utility in reproducibly distinguishing two copies of repeats from a single copy, which is not easily achievable using other standard methods. MPLA also overcomes the instability of the qPCR technique due to its high sensitivity to the amounts of template DNA, and thereby yields reproducible results[22]. Hence, MLPA is often used for the identification of deletion/duplication mutations in disease-causing genes or for determining the status of copy number variations at certain chromosomal loci in humans. In our current study, the use of MLPA allowed us to clearly determine the copy number of the integrated HHV-6B genome in the carriers and to characterize structural variations in the integrated viral genome among these CIHHV-6B cases. Our data indicate that human telomere repeats and the viral genomes had fused via one of the two TRSs within the DR-R in all six cases and

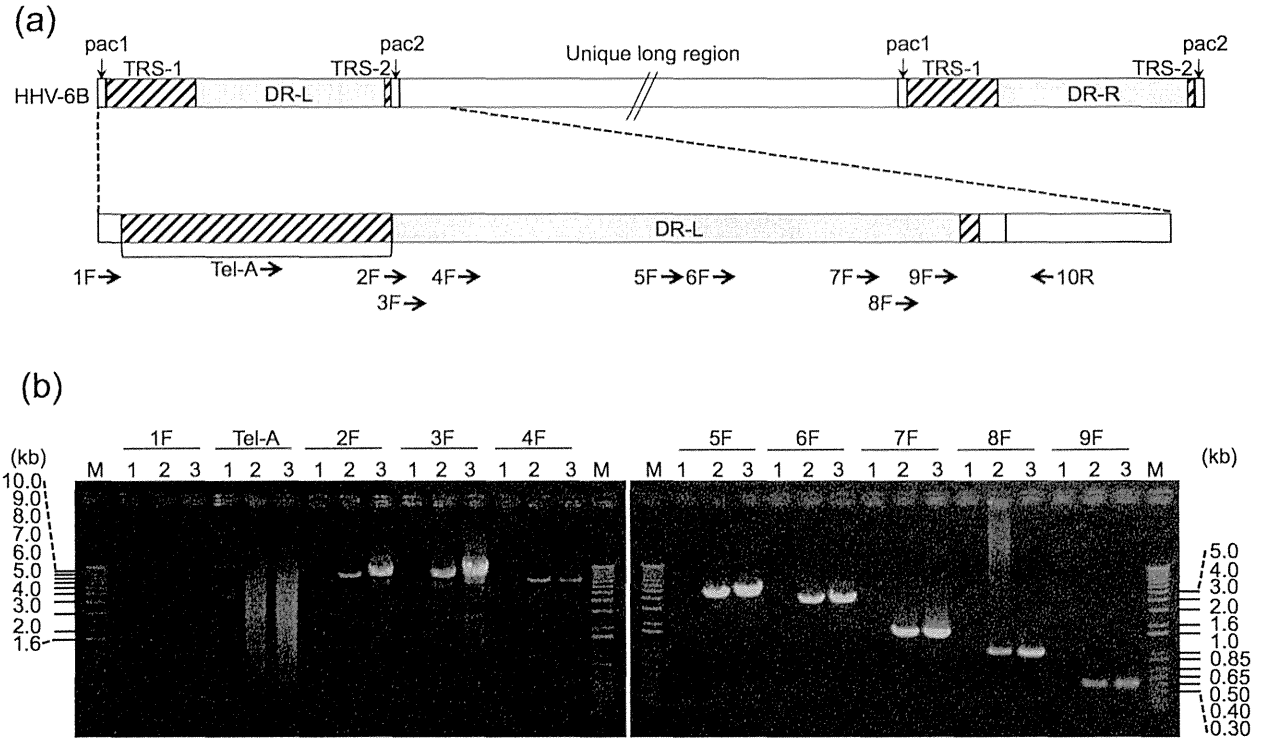

Figure 4 | Long range PCR analyses to determine the endpoints of the viral genomes. (a) Schematic representation of the HHV-6B genomic structure. The positions of the PCR primers are indicated below the diagram. (b) Results of long range PCR analyses. The 10R primer was used together with one of the DR primers for the long range PCR. The DR primers are indicated above the panels. Lane M, size markers; lane 1, non-CIHHV-6 case; lane 2, case 28; lane 3, case 18.

that the other end of the integrated HHV-6 virus is likely to be the distal TRS within the DR-L. Our findings are almost similar to those published previously[18,25]. These data implicate dual roles for the viral TRS sites in the manifestation of CIHHV-6.

The first important role of the viral TRS in the onset of CIHHV-6 is to trigger the homology-directed DNA repair mechanism for subsequent integration of the viral genome into the human genome. The ends of chromosomal DNA comprising the telomeres are generally structurally organized not to activate a DNA damage response by forming a stable T-loop DNA secondary structure and through the assembly of a shelterin complex[17]. Indeed, in normal cells, homologous recombination is repressed at the telomere[23]. However, the shortening of telomeres as a result of cell division might lead to a loss of chromosomal end protection and may cause improper DNA repair such as end-to-end fusions of the chromosomes by non-homologous end joining[24]. In our current study, the telomere repeats at the junction between the human subtelomere and the HHV-6 genome were found to be low in number, which has also been reported previously[18]. We thus speculate that telomere shortening, when it occurs in the cells infected with HHV-6, may activate a homology-directed DNA damage response that leads to viral integration.

A previous report has indicated that the viral breakpoints are located at TRS-2, both for CIHHV-6A and 6B[18,25]. The TRS-2 site has been shown to be longer and contain fewer degenerate TTAGGG repeats than TRS-1. However, our current analyses has revealed that the sizes of the TRS-1 region in our study subjects were much larger than TRS-2 and contained more perfect telomere repeats. If the free DNA end at the human telomere had activated the homology-directed DNA repair response pathway and searched for the appropriate template for DNA repair via homology, the integration event would have preferentially utilized TRS-1. However, we found that this was not the case. Thus, we speculate that the viral DNA end may be recognized as a bona fide DNA end by the host DNA repair system and thus subjected to end resection via homology-directed machinery. A small resection would be sufficient to reach the TRS-2 in the DR-R and enable the DNA end to find its homologous template, i.e. the human telomere. If the protection of the human telomere is incidentally removed at the time of this homology search due to age-related telomere shortening, the two DNA ends might be connected in a homology-dependent manner.

Once HHV-6 infection is established, the circularization of the linear double stranded viral DNA give rises to the formation of a stable episomal form in the nucleus whereby latency is achieved[26]. During HHV-6 replication, the episome produces a head-to-tail concatemer via a rolling circle mechanism, which is cleaved into a single unit of linear viral genome and is subsequently recircularized. A previous study has reported that some CIHHV individuals carry more than two copies of HHV[27]. However, in our current study we found only one copy of the viral genome in all of the CIHHV-6 cases in our cohort. In case 28, we identified tandem DRs repeat with no intervening pacl-pac2 region, which should be identified in a replicating concatemer or episomal virus. This suggests that a single linear form of replicated HHV-6 in latently infected cells gives rise to the integration event[10]. Normally, linear viral DNA ends are protected by episome formation, but it is possible that replication errors at the junction might result in an uncircularized virus genome, which may induce a DNA damage response. Although homologous recombination is suppressed at the telomere, a recent report has provided evidence of single strand annealing as a mechanism of telomere fusion[28].

The second pivotal role of the TRS regions in CIHHV-6 is the stabilization of the chromosomal end required for transmission of the virus. In our current analyses, we demonstrate that the end of the HHV-6B integrated chromosome was TRS-1, which others have also demonstrated using single telomere length analyses[25]. Once HHV-6 is integrated into the human telomere via homology with the TRS in the DR-R, the other end of the viral genome, DR-L, becomes a chromosomal end. Without the protection that normally operates

Table 1 | Characteristics of the Japanese study subjects with CIHHV-6B

Family	Case	Trigger for the diagnosis of CIHHV-6B	Chromosome
1	18	Monitoring after bone-marrow transplantation Aplastic anemia	22q
2	19	Differential diagnosis of mycoplasma Encephalitis	22q
	20	Mother of case19	22q
3	28	Monitoring after bone-marrow transplantation Congenital pure red cell aplasia	Xp
4	31	Differential diagnosis of febrile skin rash	6q
5	63	Uveitis	Xp

for chromosomal ends at the telomeres, the DR-L is subject to DNA end resection until the TRS-1 appears. Since the TRS-1 length is sufficient to recruit components of the shelterin complex, it can form a neo-telomere to maintain its size during some rounds of DNA replication and cell division until it forms gametes to transmit the viral genome to the offspring. We note that there is no reported case of chromosomally integrated HHV-7[29] and this might be due to a short TRS-1 (90 bp) in the genome of this virus which cannot maintain chromosomal end stabilization (U43400).

One of our current CIHHV-6B cases (case 31) was found to carry a different junction between the virus and human telomere, with a breakpoint in the TRS-1 region. One possibility for this occurrence is that a long DNA end resection took place that extended to the TRS1, which may be rare. Another possibility is a post-insertional genomic rearrangement[30]. Alternatively, non-allelic homologous recombination (NAHR) between the two TRS sites might have produced the deletion of DR-R in case 31, thereby mimicking the breakpoint at a different location for the initial integration. Another CIHHV-6B subject in our present analyses (case 28) was found to carry three DR copies. This is also possibly a product of an NAHR event between the two different TRS sites on the HHV-6 virus. In contrast to the normal repression of homologous recombination at the telomere, the subtelomeric region is known to be highly unstable and undergo frequent recombination[31]. The integration of HHV-6B in cases 28 and 63 in our present study are likely to have originated from a single ancestor since an identical genomic structure, three DR sites without a pac1-pac2 junction, was found in these two individuals. However, the repeat number at the TRS2-human telomere junction, as well as in the TRS2 site at the DR-L was found to be diverse between these two cases, suggesting that replication slippage or recombination may occur frequently at this new subtelomeric region.

A remaining question from our current observations is the timing of HHV-6 integration during the life cycle of a human host. Since CIHHV-6 appears to be transmitted from parent to child in a Mendelian fashion, the integration event must occur during germ cell development. HHV-6 uses CD46 as its receptor for entry into the cell[32]. Since CD46, a regulator of the complement activation receptor, is expressed ubiquitously, HHV-6 can theoretically infect all human cell types including those of a germ cell lineage. Since spermatogenic cells undergo a considerably greater number of DNA replication and cell division events than any other cells, there may be a higher chance of an integration event due to telomere dysfunction, although germ cells do possess telomerase activity[33]. Our current findings that some identified CIHHV-6 cases have similar molecular characteristics suggest that integration is a rare event. We propose from this that a small number of ancestral chromosomes that had undergone a HHV-6 integration have likely expanded throughout the general human population as a neutral polymorphism.

Methods

Human subjects. We analyzed six Japanese cases that were suspected to CIHHV-6B by having genome-equivalent copy number of viral DNA in peripheral blood samples estimated by qPCR[20]. The clinical features of the cases are listed in Table 1. After informed consent was obtained, peripheral blood samples were obtained again from each patient for our genomic analyses. Our study was approved by the Ethical Review Board for Human Genome Studies at Fujita Health University (Accession number 90, approved on 24 March 2010). All cases provided their written informed consent to participate in this study.

Fluorescent in situ hybridization (FISH). FISH was performed using a standard method. Briefly, PHA-stimulated lymphocytes or EB-transformed lymphoblasts were arrested by treatment with colcemid. Metaphase preparations were obtained by hypotonic treatment using 0.075 M KCl followed by methanol/acetate fixation. A 10 kb PstI fragment of HHV-6 was used as the probe (Fig. 1a)[3,12]. Probes were labeled by nick-translation with biotin-16-dUTP or digoxigenin-11-dUTP. After hybridization, the probes were detected using either Alexa Fluor® 488-conjugated streptavidin or rhodamine-conjugated anti-digoxigenin, respectively. Chromosomes were visualized by counter-staining with 4′,6-diamino-2-phenylindole (DAPI). As reference standards, we used RP11-186O8 (22q11.21), TelVysion 6p SpectrumGreen and TelVysion Xq/Yq SpectrumOrange (Abbott Molecular, IllinoisI, USA).

Multiplex ligation-dependent probe amplification (MLPA). MLPA probe pairs were designed using a standard methodology[22] so that they are strategically distributed throughout the viral genome, the central unique long (UL) region and two DRs, as well as pac1 and pac2. In this strategy, MLPA probes consist of two oligonucleotides, each containing a PCR primer sequence and a variable length sequence complementary to the target. Genomic DNA was denatured (1 min at 98°C) and subsequently hybridized to the MLPA probe pairs in accordance with the manufacturer's protocol (MRC-Holland, Amsterdam, Netherlands). After ligation, probe pairs were amplified using universal primers. The multiplex PCR products were then separated on a capillary sequencer. For normalization, we created a plasmid harboring a tandem array of probe sequences separated by 10-nucleotide spacer and used this construct as a standard for the copy number. We only had an EB-transformed cell line for case 63 and did not use this sample for MLPA because the presence of the EB virus genome may affect the results.

Analysis of junction fragments. Southern hybridization was performed using a standard methodology. Briefly, genomic DNA was cleaved with appropriate restriction enzymes, followed by size-separation via 0.8% agarose gel electrophoresis. After denaturation, the DNA was blotted onto a nylon membrane. Probes were labeled by crosslinking with alkaline-phosphatase and detected using CDP-Star detection reagent (GE Healthcare, Buckinghamshire, UK). To isolate a junction fragment, standard or long-range PCR was performed using LA Taq (TaKaRa, Siga, Japan). The amplification conditions were 35 cycles of 10 sec at 98°C, 30 sec at 63°C and 10 min at 72°C. A PCR primer was designed using the sequence data for the human chromosome X genomic contig (accession number NT_167191.1) and that of the HST strain of HHV-6B (AB021506). X-2R primer: 5′-TTGTCTCAGGGTCCTAGTG-3′. The PCR products were sequenced using the Sanger method.

Mapping of the distal breakpoints. To map distal breakpoints on the viral genomes, long-range PCR was performed using LA Taq. PCR primers were designed using the sequence data for the HST strain of HHV-6B (AB021506). The amplification conditions were 35 cycles of 10 sec at 98°C, 30 sec at 63°C and 10 min at 72°C. For amplification of larger fragments, PCR cycles were increased up to 38 cycles. To amplify telomere repeats, we performed the PCR using the Tel-A primer, 5′-CCCTAACCCTAACCCTAACCCTAACC-3′. To show the smear products really contain telomeric repeats Southern hybridization was performed with a telomere-specific probe[34].

1. Abtashi, D. V. *et al.* Human herpesvirus-6 strain groups: a nomenclature. *Arch Virol* **129**, 363–366 (1993).
2. Dominguez, G. *et al.* Human herpesvirus 6B genome sequence: coding content and comparison with human herpesvirus 6A. *J Virol* **73**, 8040–8052 (1999).
3. Isegawa, Y. *et al.* Comparison of the complete DNA sequences of human herpesvirus 6 variants A and B. *J Virol* **73**, 8053–8063 (1999).
4. Yamanishi, K. *et al.* Identification of human herpesvirus-6 as a causal agent for exanthem subitum. *Lancet* **1**, 1065–1067 (1988).
5. Yoshikawa, T. *et al.* Distribution of antibodies to a causative agent of exanthem subitum (human herpesvirus-6) in healthy individuals. *Pediatrics* **84**, 675–677 (1989).
6. Fox, J. D., Briggs, M., Ward, P. A. & Tedder, R. S. Human herpesvirus 6 in salivary glands. *Lancet* **336**, 590–593 (1990).

7. Kondo, K., Kondo, T., Okuno, T., Takahashi, M. & Yamanishi, K. Latent human herpesvirus 6 infection of human monocytes/macrophages. *J Gen Virol* **72 (Pt 6)**, 1401–1408 (1991).
8. Yoshikawa, T. *et al.* Human herpesvirus-6 infection in bone marrow transplantation. *Blood* **78**, 1381–1384 (1991).
9. Yoshikawa, T. Human herpesvirus 6 infection in hematopoietic stem cell transplant patients. *Br J Haematol* **124**, 421–432 (2004).
10. Morissette, G. & Flamand, L. Herpesviruses and chromosomal integration. *J Virol* **84**, 12100–12109 (2010).
11. Hall, C. B. *et al.* Chromosomal integration of human herpesvirus 6 is the major mode of congenital human herpesvirus 6 infection. *Pediatrics* **122**, 513–520 (2008).
12. Tanaka-Taya, K. *et al.* Human herpesvirus 6 (HHV-6) is transmitted from parent to child in an integrated form and characterization of cases with chromosomally integrated HHV-6 DNA. *J Med Virol* **73**, 465–473 (2004).
13. Pellett, P. E. *et al.* Chromosomally integrated human herpesvirus 6: questions and answers. *Rev Med Virol* **22**, 144–155 (2011).
14. Nacheva, E. P. *et al.* Human herpesvirus 6 integrates within telomeric regions as evidenced by five different chromosomal sites. *J Med Virol* **80**, 1952–1958 (2008).
15. Thomson, B. J., Dewhurst, S. & Gray, D. Structure and heterogeneity of the a sequences of human herpesvirus 6 strain variants U1102 and Z29 and identification of human telomeric repeat sequences at the genomic termini. *J Virol* **68**, 3007–3014 (1994).
16. Gompels, U. A. & Macaulay, H. A. Characterization of human telomeric repeat sequences from human herpesvirus 6 and relationship to replication. *J Gen Virol* **76 (Pt 2)**, 451–458 (1995).
17. de Lange, T. How telomeres solve the end-protection problem. *Science* **326**, 948–952 (2009).
18. Arbuckle, J. H. *et al.* The latent human herpesvirus-6A genome specifically integrates in telomeres of human chromosomes in vivo and in vitro. *Proc Natl Acad Sci U S A* **107**, 5563–5568 (2010).
19. Arbuckle, J. H. & Medveczky, P. G. The molecular biology of human herpesvirus-6 latency and telomere integration. *Microbes Infect* **13**, 731–741 (2011).
20. Tanaka, N. *et al.* Monitoring four herpesviruses in unrelated cord blood transplantation. *Bone Marrow Transplant* **26**, 1193–1197 (2000).
21. Achour, A. *et al.* Length variability of telomeric repeat sequences of human herpesvirus 6 DNA. *J Virol Methods* **159**, 127–130 (2009).
22. Schouten, J. P. *et al.* Relative quantification of 40 nucleic acid sequences by multiplex ligation-dependent probe amplification. *Nucleic Acids Res* **30**, e57 (2002).
23. Celli, G. B., Denchi, E. L. & de Lange, T. Ku70 stimulates fusion of dysfunctional telomeres yet protects chromosome ends from homologous recombination. *Nat Cell Biol* **8**, 885–890 (2006).
24. Celli, G. B. & de Lange, T. DNA processing is not required for ATM-mediated telomere damage response after TRF2 deletion. *Nat Cell Biol* **7**, 712–718 (2005).
25. Arbuckle, J. H. *et al.* Mapping the telomere integrated genome of human herpesvirus 6A and 6B. *Virology* **442**, 3–11 (2013).
26. Flamand, L., Komaroff, A. L., Arbuckle, J. H., Medveczky, P. G. & Ablashi, D. V. Review, part 1: Human herpesvirus-6-basic biology, diagnostic testing, and antiviral efficacy. *J Med Virol* **82**, 1560–1568 (2010).
27. Leong, H. N. *et al.* The prevalence of chromosomally integrated human herpesvirus 6 genomes in the blood of UK blood donors. *J Med Virol* **79**, 45–51 (2007).
28. Wang, X. & Baumann, P. Chromosome fusions following telomere loss are mediated by single-strand annealing. *Mol Cell* **31**, 463–473 (2008).
29. Hall, C. B. *et al.* Congenital infections with human herpesvirus 6 (HHV6) and human herpesvirus 7 (HHV7). *J Pediatr* **145**, 472–477 (2004).
30. Feschotte, C. & Gilbert, C. Endogenous viruses: insights into viral evolution and impact on host biology. *Nat Rev Genet* **13**, 283–296 (2012).
31. Linardopoulou, E. V. *et al.* Human subtelomeres are hot spots of interchromosomal recombination and segmental duplication. *Nature* **437**, 94–100 (2005).
32. De Bolle, L., Naesens, L. & De Clercq, E. Update on human herpesvirus 6 biology, clinical features, and therapy. *Clin Microbiol Rev* **18**, 217–245 (2005).
33. Kurahashi, H. *et al.* Recent advance in our understanding of the molecular nature of chromosomal abnormalities. *J Hum Genet* **54**, 253–260 (2009).
34. Ijdo, J. W., Wells, R. A., Baldini, A. & Reeders, S. T. Improved telomere detection using a telomere repeat probe (TTAGGG)n generated by PCR. *Nucleic Acids Res* **19**, 4780 (1991).

Acknowledgments

The authors thank Dr. Hiroshi Kogo and Makiko Tsutsumi for helpful discussions, Akiko Yoshikawa, Noriko Hayashizono and Narumi Kamiya for technical assistance. This work was supported by a grant-in-aid for Scientific Research from the Ministry of Education, Culture, Sports, Science, and Technology of Japan (24390085, 23659182, 23013019, http://www.mext.go.jp), and from the Ministry of Health, Labour and Welfare of Japan, to H.K (10103465, http://www.mhlw.go.jp).

Author contributions

T.O., T.Y. and H.K. conceived and designed the experiments. T.O. performed all the experiments. I.H., M.I., Y.H., K.K., J.O., H.Y., T.N., Y.T., S.K. and T.Y., contributed regents and materials. T.O. and H.K. wrote the manuscript. All authors reviewed the manuscript.

Additional information

Supplementary information accompanies this paper at http://www.nature.com/scientificreports

Competing financial interests: The authors declare no competing financial interests.

How to cite this article: Ohye, T. *et al.* Dual roles for the telomeric repeats in chromosomally integrated human herpesvirus-6. *Sci. Rep.* **4**, 4559; DOI:10.1038/srep04559 (2014).

Long-Term Parvovirus B19 Infections With Genetic Drift After Cord Blood Transplantation Complicated by Persistent CD4+ Lymphocytopenia

Michio Suzuki, MD, Yoshinori Ito, MD, PhD,* Akira Shimada, MD, PhD,* Mika Saito, PhD,† Hideki Muramatsu, MD, PhD,* Asahito Hama, MD, PhD,* Yoshiyuki Takahashi, MD, PhD,* Hirokazu Kimura, PhD,‡ and Seiji Kojima, MD, PhD**

Summary: A 5-month-old girl was diagnosed with Langerhans cell histiocytosis and received unrelated umbilical cord blood transplantation at the age of 14 months. After cord blood transplantation, CD4+ lymphocytopenia from unknown causes was observed, and persistent infections with human parvovirus B19 (B19) occurred. We performed repeated longitudinal genetic analysis for B19, which revealed 6 nucleotide mutations in B19 nonstructural protein regions in the patient. The resulting changes of the nonstructural 1 structure may have altered antigenicity of the virus and could play a role in the pathogenesis of persistent infection under immunocompromised conditions.

Key Words: cord blood transplantation, genetic drift, lymphocytopenia, parvovirus B19

(*J Pediatr Hematol Oncol* 2014;36:e65–e68)

Human parvovirus B19 (B19) is a nonenveloped, 5.5 kb, single-strand DNA virus. The virus has 2 major open reading frames, one encoding the nonstructural protein, nonstructural (NS) 1, and the other encoding the capsid proteins, viral protein (VP) 1 and VP2.[1] Three B19 genotypes (1, 2, and 3) have been described. Genotypes 2 and 3 are genetically distant from genotype 1 with nucleotide divergence of >11%.[1] Genotypes 2 and 3 are infrequently detected in clinical specimens, but the frequency was shown to be much higher in 1 prospective study. The true prevalence and clinical relevance of these differences are not fully known. In addition to causing erythema infectiosum, the B19 virus also causes arthropathy in adults, particularly in middle-aged women, aplastic crisis in patients with hemolytic anemia, chronic hypoplastic anemia in immunocompromised hosts, and fetal hydrops as a result of infection during pregnancy.[2] It has also been associated with autoimmune diseases including rheumatoid arthritis and systemic lupus erythematosus.[3] In general, infection is transient in immunocompetent patients; however, persistent infection has been reported in immunocompromised patients such as those with human immunodeficiency virus (HIV).[4] The B19 virus is a rare cause of posttransplant viral infection,[5] and there have been a few reports of persistent infections after stem cell transplantation.[6]

We report a case of persistent infections with B19 virus in a patient who developed persistent CD4+ lymphocytopenia after cord blood transplantation (CBT) for Langerhans cell histiocytosis. We studied longitudinal changes in viral DNA load and genetic changes of B19 during the course of these persistent infections.

MATERIALS AND METHODS

EDTA-treated peripheral blood was prospectively collected after transplantation for routine blood examinations and to monitor for Epstein-Barr virus, cytomegalovirus, and human herpesvirus 6 DNA until discharge. After discharge, blood samples were obtained at each patient visit for routine blood examinations. When the patient showed hemolytic anemia or after B19 DNA became positive in whole blood samples, B19 DNA was also measured. A biopsy specimen from a circumanal ulcer was also obtained when Crohn disease was suspected. DNA was extracted from 200 μL of whole blood and biopsy tissue using QIAamp blood kits (Qiagen, Hilden, Germany) and TaKaRa DEXPAT (Takara, Ohtsu, Shiga, Japan), respectively. Real-time quantitative polymerase chain reaction assay for B19 was performed as described previously.[7,8]

For genetic analysis of B19, 2 B19 viremic samples at different time points of persistent B19 infection were analyzed by DNA sequencing as described previously.[9] The primers were used for sequencing the NS1/VP1/VP2 regions. Then, B19 sequences were aligned using Clustal W (http://clustalw.ddbj.nig.ac.jp/top-j.html) for genotypic analysis. Genetic distances were calculated using the Kimura 2-parameter method,[10] and phylogenetic trees were constructed by the neighbor-joining method.[11] Results of phylogenetic trees were visualized using TreeExplorer software version 2.12 (http://www.ctu.edu.vn/~dvxe/Bioinformatic/Software/BIT%20Software/TE_man.html). Prototype B19 sequences from GenBank were used as reference sequences (accession numbers were as follows: genotype 1, M24682 [B19-Wi], M13178 [B19-Au]; genotype 2, AY064475 [B19-A6], AY044266 [B19-Wi]; genotype 3, AX003421 [B19-V9], AY083234 [B19-D91.1]).

The protocol of this study was approved by the Nagoya University Institutional Review Board, and written informed consent was obtained from the parents of the patient.

CASE REPORT

A 5-month-old girl was diagnosed with multisystem Langerhans cell histiocytosis. Although she received 2 courses of DAL

Received for publication August 22, 2012; accepted August 20, 2013.
From the *Department of Pediatrics, Nagoya University Graduate School of Medicine, Nagoya; †Gunma Prefectural Institute of Public Health and Environmental Sciences, Gunma; and ‡Infectious Disease Surveillance Center, National Institute of Infectious Diseases, Tokyo, Japan.
The authors declare no conflict of interest.
Reprints: Seiji Kojima, MD, PhD, Department of Pediatrics, Nagoya University Graduate School of Medicine, 65 Tsurumai-cho, Showa-ku, Nagoya 466-8550, Japan (e-mail: kojimas@med.nagoya-u.ac.jp).

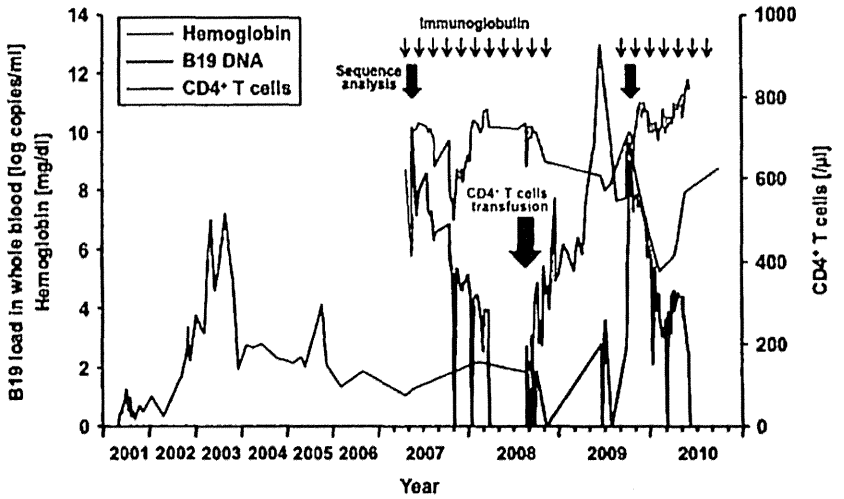

FIGURE 1. *Time course of the number of CD4+ T cells and parvovirus B19 viral load in whole blood in relation to representative laboratory data after cord blood cell transplantation. Levels of viral DNA in whole blood samples were measured by real-time quantitative polymerase chain reaction assays. Genetic analyses at the first and the second peak of viremia (black large arrows) were performed. Short arrows indicate weekly intravenous immunoglobulin treatment at 400 mg/kg/d. Blue arrow represents the time of CD4+ T-cell transfusion.*

HX-83 induction therapy, which includes prednisone, vinblastine, and etoposide, her disease did not improve. She received unrelated umbilical CBT at 14 months of age (April 2001). The conditioning regimen consisted of cyclophosphamide (60 mg/kg) on days −4 and −3; antithymocyte globulin (2.5 mg/kg) on days −5, −4, −3, and −2; and total body irradiation (2.5 Gy) twice a day on days −2 and −1. Methotrexate and tacrolimus were given for prophylaxis against graft-versus-host disease (GVHD). Neutrophil engraftment was documented on day 24 and full donor chimerism was observed after CBT; however, the number of CD4+ T cells did not go above 100/μL for 1 year after transplantation and CD4+ lymphocytopenia persisted for >7 years (Fig. 1). Her IgG, IgM, and IgA were 835, 42, and 32 mg/dL, respectively, at day 35 after transplantation. Stimulation tests with phytohemagglutinin and concanavalin A showed low responses. Natural killer cell activity was in the normal range (24%) at day 75 after transplantation. She suffered from grade 1 acute GVHD, but chronic GVHD did not develop.

She developed cough and fever at the age of 7 (May 2007). Her hemoglobin level was 5.8 g/dL and reticulocytes showed 0.4%. A bone marrow aspiration showed hypoplastic marrow with poor erythroid elements. Specific IgM antibodies for B19 were positive. B19 DNA in a whole blood sample was 1.4×10^{10} copies/mL. Underlying causes, such as thymoma, secondary cancer, drugs, and autoimmune disorders, were excluded. She received a 3-day course of intravenous immunoglobulin (400 mg/kg) daily for treatment of pure red cell aplasia. B19 viremia persisted, and the reticulocyte count did not improve, so she was treated repeatedly with 400 mg/kg/d immunoglobulin every week; she did not receive any blood transfusions. In September 2008, she was transfused with activated CD4+ T lymphocytes (3.4×10^7/kg) that were prepared from her own mononuclear cells as described previously.[12] Her CD4+ cells were over 500/μL after infusion (Fig. 1). Viremia improved slowly after weekly immunoglobulin treatment started, and this treatment was continued until January 2009 (Fig. 1). In October 2009, her reticulocyte count and hemoglobin level were 0.5% and 9 g/dL, respectively, and her level of B19 DNA was 9.8×10^8 copies/mL. Weekly immunoglobulin treatment was restarted.

She had a fever and noticed multiple oral aphtha, which became increasingly severe in January 2010. Crohn disease was suspected due to a circumanal ulcer and a red papule on the dorsal surface of the left hand, which occurred in February 2010. Histopathologic examination of biopsy samples from the ulcer showed nonspecific inflammation and B19 DNA was detected (1.49×10^5 copy/μg) in the biopsy specimen. Oral aphtha, the circumanal ulcer, and fever improved in April 2010 without any specific treatment besides weekly immunoglobulin treatment. B19 DNA disappeared in June 2010.

RESULTS AND DISCUSSION

Cytomegalovirus, Epstein-Barr virus, and herpes simplex virus are common causes of posttransplantation viral infection, whereas infection with B19 virus is rare after hematopoietic stem cell transplantation. The incidence of primary or recurrent infection with B19 in patients after allogenic hematopoietic stem cell transplantation seems to be 1% to 2%.[13] Eid et al[5] investigated 98 cases of posttransplantation B19 infection, including 24 cases after hematopoietic stem cell transplantation. Anemia was observed in 98.8% of patients with B19 infection. Fever and flu-like manifestations occurred in 25.9% of patients and skin rash occurred in 13.3% of patients. B19 infection occurred between 1 week and 96 months after transplantation, with a

TABLE 1. *Nucleotide Substitutions Found in Longitudinal Isolates*

	Nucleotide					
	941	**1037**	**1048**	**1112**	**1118**	**1266**
Date						
May 24, 2007	T/C	T/C	A	T	T	A
October 19, 2009	T	T	A/G	C	T/C	A/G
Amino acid change			K→K/R			T→T/A

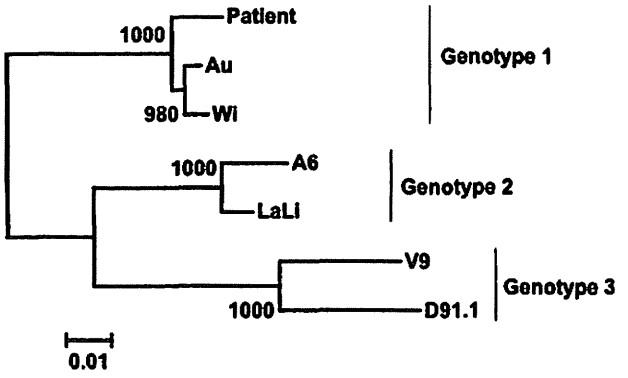

FIGURE 2. Phylogenetic tree constructed from VP1 sequence. The HPV B19 sequence from the patient was aligned with reference sequences by GenBank (genotype 1, B19-Wi and B19-Au; genotype 2, B19-A6 and B19-Wi; genotype 3, B-19-V9 and B19-D91.1). Genetic distances were calculated using the Kimura 2-parameter method and phylogenetic trees were constructed using the neighbor-joining method.

median onset time of 1.8 months. Recurrence of B19 infection occurred in 23% of cases. In the present case, onset occurred 76 months after CBT, causing symptomatic persistent infection for >3 years. Repeated administration of immunoglobulin was effective and B19 DNA disappeared. However, anemia and B19 viremia may recur, because CD4+ lymphocytopenia has not been cured.

B19 infection is known to cause persistent pure red-cell aplasia in immunocompromised patients in whom B19 virus-specific antibody production is insufficient.[2,14] Previous reports have described persistent infection with B19 in patients with congenital immunodeficiency syndrome,[2] patients receiving cytotoxic chemotherapy or immunosuppressive drugs,[2] patients undergoing bone marrow transplantation[5,6] or organ transplantation,[5] and patients with HIV infection.[4] In the present case, persistent CD4+ lymphocytopenia of unknown cause was present after transplantation, which likely caused the subsequent persistent B19 infection. CD4 deficiency has been shown to be present in HIV infection and idiopathic CD4+ lymphocytopenia, in which opportunistic infections can occur. Cryptococcus is one of the more common infections in patients with CD4 penia.[15] Zonios et al[16] reported that cryptococcal and nontuberculous mycobacterial infections were the major presenting opportunistic infections of idiopathic CD4+ lymphocytopenia in 33.3% (13/39) and 20.5% (8/39) of cases, respectively. Infections caused by cytomegalovirus, Epstein-Barr virus, human herpesvirus 8, human papillomavirus, JC virus, and varicella zoster virus were reported in a small number of cases.[16] The present case suffered from long-standing infections with B19, and this pathogen is rare in a patient with idiopathic CD4+ lymphocytopenia.

To our knowledge, this is the first report of idiopathic CD4+ lymphocytopenia after hematopoietic stem cell transplantation. The treatment of idiopathic CD4+ lymphocytopenia mainly consists of prophylaxis and treatment of opportunistic infections and attempts to increase CD4+ T-cell counts. Interleukin-2 therapy is an option to increase CD4+ counts along with other cytokines such as interferon-γ and interleukin-7.[15] Hematopoietic stem cell transplantation may be another treatment option to restore CD4+ T-cell count and immune function in idiopathic CD4+ lymphocytopenia.[17] The present case is an unfavorable example of hematopoietic stem cell transplantation as a cause.

To characterize B19 in this patient, sequence analysis of the coding regions of 3 major B19 proteins, that is, NS1, VP1, and VP2, in blood samples was performed. Analyses at the first and the second peak of viremia (Fig. 1) revealed sequence variations at 6 positions in the NS1 area; 2 of them were nonsynonymous mutations, which altered the amino acid sequence of the protein (Table 1). These changes may have influenced the protein structure and biological function of NS1, thus affecting the course of infection. NS1 protein is known to be cytotoxic and also autoregulates its own transcription, which may affect synthesis of NS1 protein.[18] In addition, changes in the NS1 protein structure may alter antigenicity and the recognition of humoral antibodies that confer resistance to immunoglobulin infusions. This patient received intravenous immunoglobulin for treatment of B19 infection, and these genetic changes may have been caused by selection of resistant clones, although direct evidence of this selection was not shown in the present study. Further studies are needed to clarify the effects that arise from amino acid changes. Although B19 is usually stable genetically, and mutations seldom occur during the course of infection, genetic drift of B19 in acquired immunodeficiency syndrome patients with CD4 lymphocytopenia has been reported.[1]

Phylogenic analysis on the basis of the VP1 region, which was identical between the 2 different samples, revealed that this B19 virus was identified as genotype 1 (Fig. 2), which usually causes acute and transient infection.[19] Servant et al[19] reported that most genotype 2 and 3 viruses were isolated in patients older than those infected with genotype 1 virus, frequently in association with immunodeficiency. They hypothesized that adult patients with impaired immunity, who are likely to have experienced a previous genotype 1 virus infection, might be reinfected by a genotype 2 or 3 virus. However, the current patient had no blood transfusions and had been kept in the hospital, suggesting that superinfection of another B19 was not likely. B19 infections are ubiquitous and can cause an asymptomatic infection including a mild respiratory tract illness with no rash. The index case is generally unrecognized in nosocomial infections.[20] Therefore, identification of the source of B19 infection is usually difficult.

In this case report, idiopathic CD4+ lymphocytopenia was unexpectedly observed after CBT, and infections with B19 persisted for several years. The resulting changes of the NS1 during persist infection may have altered antigenicity of the virus and could have played a role in the pathogenesis of persistent B19 infection under CD4+ lymphocytopenia.

REFERENCES

1. Hung CC, Sheng WH, Lee KL, et al. Genetic drift of parvovirus B19 is found in AIDS patients with persistent B19 infection. *J Med Virol.* 2006;78:1374–1384.
2. Young NS, Brown KE. Parvovirus B19. *N Engl J Med.* 2004;350:586–597.
3. Lunardi C, Tinazzi E, Bason C, et al. Human parvovirus B19 infection and autoimmunity. *Autoimmun Rev.* 2008;8:116–120.
4. Frickhofen N, Abkowitz JL, Safford M, et al. Persistent B19 parvovirus infection in patients infected with human

immunodeficiency virus type 1 (HIV-1): a treatable cause of anemia in AIDS. *Ann Intern Med.* 1990;113:926–933.
5. Eid AJ, Brown RA, Patel R, et al. Parvovirus B19 infection after transplantation: a review of 98 cases. *Clin Infect Dis.* 2006;43:40–48.
6. Plentz A, Hahn J, Holler E, et al. Long-term parvovirus B19 viraemia associated with pure red cell aplasia after allogeneic bone marrow transplantation. *J Clin Virol.* 2004; 31:16–19.
7. Shibata Y, Kitajima N, Kawada J, et al. Association of cytomegalovirus with infantile hepatitis. *Microbiol Immunol.* 2005;49:771–777.
8. Wada K, Kubota N, Ito Y, et al. Simultaneous quantification of Epstein-Barr virus, cytomegalovirus, and human herpesvirus 6 DNA in samples from transplant recipients by multiplex real-time PCR assay. *J Clin Microbiol.* 2007;45:1426–1432.
9. Toan NL, Duechting A, Kremsner PG, et al. Phylogenetic analysis of human parvovirus B19, indicating two subgroups of genotype 1 in Vietnamese patients. *J Gen Virol.* 2006;87: 2941–2949.
10. Kimura M. A simple method for estimating evolutionary rates of base substitutions through comparative studies of nucleotide sequences. *J Mol Evol.* 1980;16:111–120.
11. Saitou N, Nei M. The neighbor-joining method: a new method for reconstructing phylogenetic trees. *Mol Biol Evol.* 1987; 4:406–425.
12. Tomizawa D, Aoki Y, Nagasawa M, et al. Novel adopted immunotherapy for mixed chimerism after unrelated cord blood transplantation in Omenn syndrome. *Eur J Haematol.* 2005;75:441–444.
13. Hayes-Lattin B, Seipel TJ, Gatter K, et al. Pure red cell aplasia associated with parvovirus B19 infection occurring late after allogeneic bone marrow transplantation. *Am J Hematol.* 2004;75:142–145.
14. Anderson MJ, Higgins PG, Davis LR, et al. Experimental parvoviral infection in humans. *J Infect Dis.* 1985;152:257–265.
15. Luo L, Li T. Idiopathic CD4$^+$ lymphocytopenia and oppotunistic infection - an update. *FEMS Immunol Med Microbiol.* 2008;54:283–289.
16. Zonios DI, Falloon J, Bennett JE, et al. Idiopathic CD4$^+$ lymphocytopenia: natural history and prognostic factors. *Blood.* 2008;112:287–294.
17. Petersen EJ, Rozenberg-Arska M, Dekker AW, et al. Allogenic bone marrow transplantation can restore CD4$^+$ T-lymphocyte count and immune function in idiopathic CD4$^+$ T-lymphocytopenia. *Bone Marrow Transplant.* 1996;18:813–815.
18. Hemauer A, von Poblotzki A, Gigler A, et al. Sequence variability among different parvovirus B19 isolates. *J Gen Virol.* 1996;77:1781–1785.
19. Servant A, Laperche S, Lallemand F, et al. Genetic diversity within human erythroviruses: identification of three genotypes. *J Virol.* 2002;76:9124–9134.
20. Cherry DJ, Schulte DJ. Human parvovirus B19. In: Feigin RD, Cherry JD, Demmler-Harrison GJ, Kaplan SL, eds. *Feigin and Cherry's Textbook of Pediatric Infectious Diseases.* 6th ed. Philadelphia: Saunders; 2009:1902–1920.

PLOS | ONE

Development and Customization of a Color-Coded Microbeads-Based Assay for Drug Resistance in HIV-1 Reverse Transcriptase

Lijun Gu[1,2], Ai Kawana-Tachikawa[3], Teiichiro Shiino[4], Hitomi Nakamura[5,6], Michiko Koga[3,6], Tadashi Kikuchi[3,6], Eisuke Adachi[6], Tomohiko Koibuchi[6], Takaomi Ishida[1,2], George F. Gao[7], Masaki Matsushita[8], Wataru Sugiura[4], Aikichi Iwamoto[1,3,5,6], Noriaki Hosoya[3,5]*

1 Research Center for Asian Infectious Diseases, the Institute of Medical Science, the University of Tokyo, Tokyo, Japan, **2** Japan-China Joint Laboratory of Molecular Immunology and Molecular Microbiology, Institute of Microbiology, Chinese Academy of Sciences, Beijing, P. R. China, **3** Division of Infectious Diseases, Advanced Clinical Research Center, the Institute of Medical Science, the University of Tokyo, Tokyo, Japan, **4** AIDS Research Center, National Institute of Infectious Diseases, Tokyo, Japan, **5** Department of Infectious Disease Control, International Research Center for Infectious Diseases, the Institute of Medical Science, the University of Tokyo, Tokyo, Japan, **6** Division of Infectious Diseases and Applied Immunology, Research Hospital, The Institute of Medical Science, The University of Tokyo, Tokyo, Japan, **7** CAS Key Laboratory of Pathogenic Microbiology and Immunology, Institute of Microbiology, Chinese Academy of Sciences, Beijing, P. R. China, **8** Biotech Research and Development, Wakunaga Pharmaceutical Corporation, Hiroshima, Japan

Abstract

Background: Drug resistance (DR) of HIV-1 can be examined genotypically or phenotypically. Although sequencing is the gold standard of the genotypic resistance testing (GRT), high-throughput GRT targeted to the codons responsible for DR may be more appropriate for epidemiological studies and public health research.

Methods: We used a Japanese database to design and synthesize sequence-specific oligonucleotide probes (SSOP) for the detection of wild-type sequences and 6 DR mutations in the clade B HIV-1 reverse transcriptase region. We coupled SSOP to microbeads of the Luminex 100 xMAP system and developed a GRT based on the polymerase chain reaction (PCR)-SSOP-Luminex method.

Results: Sixteen oligoprobes for discriminating DR mutations from wild-type sequences at 6 loci were designed and synthesized, and their sensitivity and specificity were confirmed using isogenic plasmids. The PCR-SSOP-Luminex DR assay was then compared to direct sequencing using 74 plasma specimens from treatment-naïve patients or those on failing treatment. In the majority of specimens, the results of the PCR-SSOP-Luminex DR assay were concordant with sequencing results: 62/74 (83.8%) for M41, 43/74 (58.1%) for K65, 70/74 (94.6%) for K70, 55/73 (75.3%) for K103, 63/73 (86.3%) for M184 and 68/73 (93.2%) for T215. There were a number of specimens without any positive signals, especially for K65. The nucleotide position of A2723G, A2747G and C2750T were frequent polymorphisms for the wild-type amino acids K65, K66 and D67, respectively, and 14 specimens had the D67N mutation encoded by G2748A. We synthesized 14 additional oligoprobes for K65, and the sensitivity for K65 loci improved from 43/74 (58.1%) to 68/74 (91.9%).

Conclusions: We developed a rapid high-throughput assay for clade B HIV-1 DR mutations, which could be customized by synthesizing oligoprobes suitable for the circulating viruses. The assay could be a useful tool especially for public health research in both resource-rich and resource-limited settings.

Citation: Gu L, Kawana-Tachikawa A, Shiino T, Nakamura H, Koga M, et al. (2014) Development and Customization of a Color-Coded Microbeads-Based Assay for Drug Resistance in HIV-1 Reverse Transcriptase. PLoS ONE 9(10): e109823. doi:10.1371/journal.pone.0109823

Editor: Nicolas Sluis-Cremer, University of Pittsburgh, United States of America

Received May 7, 2014; **Accepted** September 10, 2014; **Published** October 14, 2014

Data Availability: The authors confirm that all data underlying the findings are fully available without restriction. All relevant data are within the paper.

Funding: This work was supported in part by a contract research fund from the Ministry of Education, Culture, Sports, Science and Technology (MEXT) for Program of Japan Initiative for Global Research Network on Infectious Diseases (10005010)(AI); Global COE Program (Center of Education and Research for Advanced Genome-Based Medicine - For personalized medicine and the control of worldwide infectious diseases -) of MEXT (F06)(AI); JSPS KAKENHI (25293226)(AKT); JSPS KAKENHI (24790437, 26860300)(NH);Grants for AIDS research from the Ministry of Health, Labor, and Welfare of Japan (H24-AIDS-IPPAN-008)(AKT); Grants for AIDS research from the Ministry of Health, Labor, and Welfare of Japan (H25-AIDS-IPPAN-006)(NH); Research on international cooperation in medical science, Research on global health issues, Health and Labour Science Research Grants, the Ministry of Health, Labor, and Welfare of Japan (H25-KOKUI-SITEI-001)(AI). The funders had no role in study design, data collection and analysis, decision to publish, or preparation of the manuscript.

Competing Interests: A.I. has received grant support from Toyama Chemical Co. Ltd., astellas, ViiV Healthcare K.K., MSD K.K., Baxter through the University of Tokyo. A.I. has received speaker's honoraria/payment for manuscript from Eiken Chemical Co. Ltd., astellas, Toyama Chemical Co. Ltd, Torii Pharmaceutical Co. Ltd., Takeda Pharmaceutical Co. Ltd. and MSD. MM is an employee of Wakunaga Pharmaceutical Corporation which keeps a patent on PCR amplification sequence-specific oligonucleotide probes (SSOP) method. For the remaining authors none were declared. This does not alter the authors' adherence to PLOS ONE policies on sharing data and materials.

* Email: hnori@ims.u-tokyo.ac.jp

Introduction

Since combination antiretroviral therapy (cART) was introduced, the prognosis of patients with HIV-1 infection has improved dramatically [1,2]. In resource-rich settings, new classes, new drugs or new formulations of previously-known classes of antiretroviral drugs (ARV) have been introduced continuously for clinical use. Nucleoside/nucleotide reverse transcriptase inhibitor (NRTI) resistance has declined over time in resource-rich settings, presumably reflecting the improvement of treatment regimens [3,4]. Rates of transmitted HIV-1 drug resistance (DR) have remained limited also in resource-limited settings; however, limitation of the first-line and subsequent regimens would be a concern. cART consisting of two NRTIs and one non-nucleoside reverse transcriptase inhibitors (NNRTI), most often zidovudine (AZT) + lamivudine (3TC) or stavudine (d4T) + 3TC plus nevirapine (NVP) or efavirenz (EFV), has been widely used as the treatment regimen in the resource-limited settings [5,6]; consequently, DR might become a larger public health challenge in the developing countries.

DR can be examined genotypically or phenotypically [7] (http://www.aidsmap.com/pdf/Resistance-tests/page/1044559/). Although sequencing is the gold standard of the genotypic resistance testing (GRT), high-throughput GRT targeted to the codons responsible for DR may be more convenient and suitable for public health research [8,9]. We applied the PCR-SSOP-Luminex method [10–12] to an HIV-1 GRT. As an initial approach, we focused on designing an assay for six major DR mutations: M41L, K65R, K70R, K103N, M184V and T215Y/F. M41L, K70R, T215F/Y are examples of thymidine analogue mutations (TAMs) and associated with AZT and d4T [13] (HIV Drug resistance database, Stanford University, http://hivdb.stanford.edu/index.html). K65R is associated multi-nucleoside and nucleotide DR. Although K65R is selected by nucleotide reverse transcriptase inhibitor tenofovir (TDF) usually, it can be selected by d4T. K103N is highly associated with EFV and NVP resistance. The K103N mutation reduces susceptibility to NVP by 50-flod, and EFV by 20-fold. M184V is highly associated with 3TC and emtricitabine (FTC) resistance, and reduce the susceptibility to 3TC by 200-fold. The monitoring of these six DR mutations should be important for molecular epidemiologic study estimating the efficacy of anti-HIV drugs especially in resource limited settings. We synthesized the oligonucleotides for the primers and probes based on the Japanese data base on reverse transcriptase mutations. In order to validate the initial assay system and examine the flexibility for customization, we focused on the clade B HIV-1 which is most prevalent in Japan. Here we report the results of the comparison between sequencing and the PCR-SSOP-Luminex assay using the specimens of a Japanese cohort.

Methods

PCR-SSOP-Luminex assay

HIV-1 DR genotyping described here is based on the reverse SSOP method coupled with a microsphere beads array platform (Luminex Corporation, Austin, TX, USA). Briefly, the method involves PCR amplification by biotinylated primers, hybridization to nucleotide probes coupled to microbeads, detection of the bound PCR products by streptavidin-phycoerythrin (SAPE) reaction, and quantitation by measurement of median fluorescence intensity (MFI).

Color-coded microbeads were coupled to oligoprobes derived from DR mutations or conserved sequences in HIV-1 RT coding region. These synthesized probes were modified at the 5′-end with a terminal amino group and covalently bound to the carboxylated fluorescent microbeads using ethylene dichloride (EDC), following the procedures recommended by the manufacturer (Wakunaga Pharmaceutical Co. Ltd, Hiroshima, Japan). Briefly, 6.25×10^5 carboxylated microbeads were suspended in 50 μl of 0.1 M MES (2-(N-morpholino) ethane sulfonic acid, pH 4.5 (Dojindo Laboratories, Kumamoto Techno Research Park, Kumamoto, Japan). Afterwards, 0.5 μM of amine-substituted oligonucleotide probes was added, followed by 100 mg/ml EDC (1-Ethyl-3-(3-dimethylaminopropyl) carbodiimido hydrochloride) (Pierce Biotechnology, Rockford, IL, USA), and the mixture was incubated in the dark for 30 min at 25°C. The EDC addition and incubation were repeated twice and the microbeads were washed once with 0.02% Tween-20 and once with 0.1% SDS. After the final wash, the pellets were resuspended in 50 μl TE buffer (pH 8.0), and counted on a hemocytometer. The concentration of fluorescence-labeled microbeads coupled to oligonucleotide probes (oligobeads) was adjusted to 8000–12000/μl, and oligobeads were stored at 4°C in the dark.

Five-microliter aliquots of the 5′-biotinlabeled amplified DNA were added to wells in a 96-well PCR tray containing 5 μl/well of denaturation solution, and allowed to denature for 5 min at RT. Hybridization mixture was prepared using oligobeads stocks, SAPE and hybridization solution, according to the manufacturer's instructions (Wakunaga Pharmaceutical Co. Ltd, Hiroshima, Japan). Twenty-five-microliter aliquots of hybridization mixture containing 500 each sequence-specific oligobeads were added to each well. The amplicons were hybridized at 55°C for 30 min using the thermal cycler. Hybridized amplicons were washed twice with 75 μl of wash solution in each well. Reaction outcomes were measured by the Luminex 100 flow cytometer that is equipped with two types of lasers. The bead populations were detected and identified using the 635 nm laser. The SAPE fluorescence of the biotin labeled amplicons that had hybridized to the oligobeads was quantitated using the 532 nm laser. The MFI of SAPE was used to quantify the amount of DNA bound to the oligobeads. Assays were performed in triplicate.

Site-directed mutagenesis and plasmid construction

To assess the feasibility of the assay system, we chose cloned SF2 genome (GenBank accession number K02007) as a template. Synthesized PCR fragments with DR mutations created by site-directed mutagenesis were inserted into the SF2 genome. The numbering system used to refer to DR mutations was based on HXB2 genome (HXB2 location 2485–3309, GenBank accession number K03455) sequences. The SF2 and HXB2 genome had the same sequence in the regions covered by the probes.

Plasmid p9B/R7 from the HIV-1 SF2 strain was a kind gift of Dr. T. Shioda (Osaka University, Osaka, Japan) [14,15]. An *Xho* I- *BamH* I fragment including the pol gene from p9B/R7 was subcloned into pBluescript II SK (+) (Stratagene, La Jolla, CA, USA). As shown in Fig. 1A, various DR mutations were introduced into the *Xho* I- *BamH* I fragment of the plasmid by site-directed mutagenesis using oligonucleotides and PCR methods as previously described [16], and were confirmed by sequencing.

Clinical specimens

Sixty subjects were selected from among patients participating in an ongoing study on microbes at an HIV outpatient clinic affiliated with the Institute of Medical Science, the University of Tokyo (IMSUT). The study was approved by the internal review board of IMSUT (20-31-1120), and all subjects provided written informed consent. The median HIV-1 RNA and CD4 cells count

A

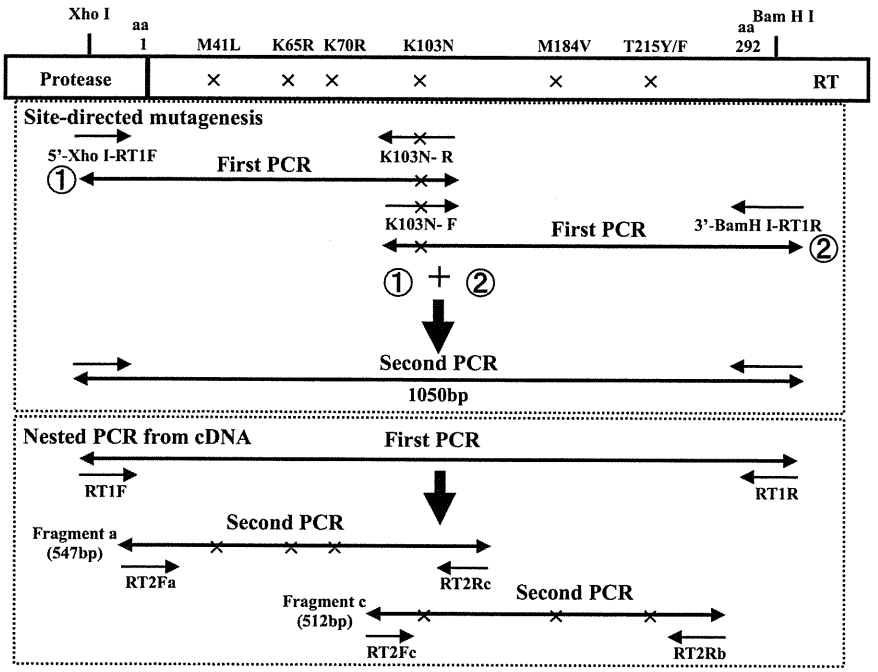

B

PCR primers

RT1F: 5'-ATGATAGGGGGAATTGGAGGTTT- 3'

RT1R: 5'- TACTTCTGTTAGTGCTTTGGTTCC- 3'

RT2Fa: 5'- GACCTACACCTGTCAACATAATTGG- 3'

RT2Rc: 5'- TGGAATATTGCTGGTGATCC- 3'

RT2Fc: 5'-AACTCAAGACTTCTGGGAAGT- 3'

RT2Rb: 5'-CAGTCCAGCTGTCTTTTTCTGGC- 3'

Sequencing primers

T7: 5′-TAATACGACTCACTATAGGG-3′

Rev: 5′-CAGGAAACAGCTATGAC-3′

Figure 1. Schematic representation of PCR amplification and sequences of primers for PCR and sequencing. (A) Top: Site-directed mutagenesis using oligonucleotide is shown using K103N as an example. Desired mutations in the reverse transcriptase gene were engineered in two PCR fragments, then incorporated into a larger fragment (1050 bp, HXB2 location 2388–3425) by the second PCR, and cloned into pBluescript II SK (+) at *Xhol-BamHI* sites. Bottom: Negative strand cDNA was synthesized from patients' plasma. After the first strand PCR using RT1F and RT1R as primers, Fragment a or Fragment c were amplified by nested PCR. (B) Primer sequences for PCR amplification and sequencing.
doi:10.1371/journal.pone.0109823.g001

at sampling were 4.15 (range 2.60–5.88) log 10 copies/ml and 264 (range: 9–902) cells/μl, respectively. Seventy-four specimens from 60 patients were analyzed in this study. Forty-eight patients contributed one plasma specimen, 10 patients contributed two plasma specimens from different time points, and two patients contributed three separate plasma specimens. Twenty-two specimens were from patients who were treatment-naïve when the plasma specimens were obtained. The remaining 52 specimens were from patients on failing treatment including NRTI at the time of sample collection.

Viral RNA extraction, cDNA synthesis, and PCR amplification

Viral RNA was extracted from 140 μl plasma using QIAamp Viral RNA Mini Kit (QIAGEN, Valencia, CA, USA) and eluted

Table 1. Design of oligoprobes based on clade B HIV-1 sequences from Japanese surveillance database.

Locus	genetic code	Frequency(%)	Name of probe	Oligoprobes	Nucleotide sequence (5'-3')	100% match isolates of database
M41					TGT ACA GAA ATG GAA	
	M41-ATG	795/795(100)	M41M-ATG	GTACAGAAATGGAA	— — — — —	618/868(71.2%)
	M41L-TTG	109/180(60.6)	M41L-TTG	GTACAGAATTGGAA	— — — T— —	
	M41L-CTG	69/180(38.3)	M41L-CTG	GTACAGAACTGGAA	— — — C— —	
	M41L-TTA	1/180(0.6)				
	M41L-TTR	1/180(0.6)				
K65					ATA AAG AAA AAA GAC AGT	
	K65-AAA	961/1012(95.0)	K65K-AAA	ATAAAGAAAAAAGACAG	— — — — — — —	516/870(59.3%)
	K65-AAG	30/1012(3.0)				
	K65-AAR	21/1012(2.1)				
	K65R-AGA	7/7(100)	K65R-AGA	ATAAAGAGAAAAGACAG	— — -G- — — —	
	K65R-AGG	0/7(0.0)				
K70					GAC AGT ACT AAA TGG AGA	
	K70-AAA	849/885(95.9)	K70K-AAA-1	GACAGTACTAAATG	— — — — —	621/769(80.8%)
			K70K-AAA-2	GTACTAAATGGAGA	— — — — —	
	K70-AAG	17/885(1.9)				
	K70-AAR	19/885(2.1)				
	K70R-AGA	85/88(96.6)	K70R-AGA	GTACTAGATGGAGA	— — -G- — —	
	K70R-AGG	0/88(0.0)	K70R-AGG	GTACTAGGTGGAGA	— — -GG — —	
	K70R-AGR	3/88(3.4)				
K103					TTA AAA AAG AAA AAA TCA GTA	
	K103-AAA	815/867(94.0)	K103K-AAA	AAAAAAGAAAAAATCAG	- — — — — — -	558/785(71.1%)
	K103-AAG	25/867(2.9)				
	K103-AAR	27/867(3.1)				
	K103N-AAC	112/128(87.5)	K103N-AAC	AAAAAAGAACAAATCAG	- — — —C — — -	
	K103N-AAT	3/128(2.3)	K103N-AAT	AAAAAAGAATAAATCAGT	- — — —T — — —	
	K103N-AAY	13/128(10.2)				
M184					TAT CAA TAC ATG GAT GAT	
	M184-ATG	659/659(100)	M184M-ATG	TATCAATACATGGATG	— — — — — -	761/888(85.7%)
	M184V-GTG	295/335(88.1)	M184V-GTG	TATCAATACGTGGATG	— — — G— — -	
	M184V-GTA	14/335(4.2)				
	M184V-GTR	26/335(7.8)				
T215					TGG GGA TTT ACC ACA CCA	
	T215-ACC	692/724(95.6)	T215T-ACC-1	GGGGATTTACCACA	— — — — —	583/813(71.7%)
			T215T-ACC-2	GGGGATTTACCACACCA	— — — — — —	
	T215-ACT	13/724(1.8)				
	T215-ACA	7/724(1.0)				
	T215-ACG	3/724(0.4)				
	T215-ACY	8/724(1.1)				
	T215-ACM	1/724(0.1)				
	T215F-TTC	54/54(100)	T215F-TTC	GGGGATTTTTCACAC	— — — TT- —	
	T215Y-TAC	182/185(98.4)	T215Y-TAC	GGGGATTTTACACAC	— — — TA- — -	
	T215Y-TAT	2/185(1.1)				
	T215Y-TAY	1/185(0.5)				
Standard probes			S2582	ATTAAAGCCAGGAATGGAT		
			S2693	AAAAATTGGGCCTGAAAAT		
			S3230	CCTTTGGATGGGTTATGAA		
			S3252	CATCCTGATAAATGGACAG		

Table 1. Cont.

Locus	genetic code	Frequency(%)	Name of probe	Oligoprobes	Nucleotide sequence (5'-3')	100% match isolates of database
			S3243	TATGAACTCCATCCTGA		

R: Mixed base of A and G; Y: Mixed base of C and T; M: Mixed base of C and A.
doi:10.1371/journal.pone.0109823.t001

with 60 μl AVE buffer. For cDNA synthesis, 55 μl of RNA solution was mixed with 5 μl of 100 pmol/μl random primer (TaKaRa Bio, Otsu, Shiga, Japan) or specific primer, RT1R (Fig. 1B), and 5 μl of 10 mM dNTPs, and denatured at 70°C for 10 min. The RT mixture containing 20 μl of 5× First-Strand buffer, 5 μl of 0.1 M DTT, 5 μl of RNaseOUT Recombinant RNase inhibitor (40 U/μl; Invitrogen, Carlsbad, California, USA) and 5 μl of SuperScript III RT (200 U/μl, Invitrogen) was added to the 65 μl denatured viral RNA-primer-dNTP mixture. The reaction mixture (100 μl final volume) was incubated at 25°C for 5 min for annealing and then at 55°C for 60 min for reverse transcription. The reaction was inactivated by heating at 70°C for 15 min.

RT gene fragments were amplified by nested PCR from cDNAs or by single PCR from plasmids. For the first reaction a 1050 bp fragment from the RT coding region was amplified from 5 μl aliquots of cDNAs using RT1F and RT1R as outer primers in a reaction mixture containing 50 μl of 1×Prime STAR buffer, 0.2 mM of each dNTPs, 0.5 μM of each primer, and 0.5 μl Prime STAR HS DNA Polymerase (25 U/μl, TaKaRa Bio, Otsu, Shiga, Japan). Amplification conditions consisted of 35 cycles denaturation at 98°C for 10 s, annealing at 55°C for 5 s, and extension at 72°C for 30 s.

For the second reaction of the nested PCR and for the single PCR from plasmids (0.1 pg), RT coding fragments were amplified in two PCR fragments using two 5′ biotinylated primer sets, PS1 and PS2, as described previously [17]. The PS1 primer set produced a 547 bp amplicon that was used to detect M41L, K65R, K70R, and K103N, and the PS2 primer set produced a 512 bp amplicon that was used to detect K103N, M184V, and T215Y/F (Fig. 1A). The reaction mixture used 5 μl of the first PCR products or 0.1 pg of plasmid DNA in a final volume of 50 μl, as described above, with amplification conditions as follows: 25 cycles (second nested PCR) or 35 cycles (plasmid DNA amplification) of denaturation at 98°C for 10 s, annealing at 55°C for 5 s, and extension at 72°C for 1 min. The PCR amplicons were used for Luminex detection or direct sequencing.

Sequencing

PCR products were purified with the QIAquick PCR Purification Kit (QIAGEN, Valencia, CA, USA) and were directly sequenced in both directions using ABI 3130xl genetic analyzer (Applied Biosystems, Foster City, CA, USA) and Big Dye terminator V3.1 cycle sequencing kit (Applied Biosystems). In the case of sequence ambiguity due to a coexistence of multiple nucleotides, we confirmed the sequence by cloning and sequencing. For cloning and sequencing, the purified PCR fragments were phosphorylated using T4 polynucleotide kinase (TaKaRa Bio, Otsu, Shiga, Japan) and inserted into the dephosphorylated *EcoR*V restriction site of pBluescript II SK(+). Inserts were sequenced using T7 and Rev universal primers (Fig. 1B).

HIV-1 Japanese surveillance database

In Japan 10 university hospitals, 5 medical centers, 5 public health laboratories, and the National Institute of Infectious Diseases are collaborating in the surveillance of newly diagnosed HIV/AIDS cases. HIV/AIDS patients with both acute and chronic infections, newly diagnosed at these centers since January 2003 were enrolled [18]. Prevalence of DR codons in these patients was determined by analysis of sequences of clade B HIV-1 reverse transcriptase positions 1–240 amino acids.

Statistical analysis

GraphPad Prism 5.0 software (GraphPad Software Inc., San Diego, CA) was used for statistical data analysis. Statistical significance was defined as $P<0.05$.

Results

Design of oligoprobes based on the database of clade B HIV-1 sequences in Japan

Based on the frequency of the codon usage in the Japanese surveillance database for amino acids M41, K65, K70, K103, M184 and T215 in RT gene, we designed the nucleotide sequence of 18 oligoprobes for DR mutation and 5 standard probes (Table 1). We adopted nucleotide sequences of HXB2 strain for the flanking sequences. Synthesized oligoprobes could cover 71.2%, 59.3%, 80.8%, 71.1%, 85.7% and 71.7% of M41, K65, K70, K103, M184 and T215, respectively (Table 1). Five standard probes were designed in the conserved region of RT gene and used as the assay control.

Evaluation of PCR-SSOP-Luminex DR assay using cloned HIV-1

We examined the sensitivity and specificity of the PCR-SSOP-Luminex DR assay using cloned HIV-1. The test fragments were amplified (Fig. 2A), and the amplicons were hybridized to the 16 oligobeads. We performed three independent assays with triplicate hybridization and detection in each assay. The mean positive signal and standard deviation were 5237±1398 (Fig. 2B). The CV% of positive signal and standard deviation were 10.1% ±10.7. The mean of negative signal and standard deviation were 131.2±69.4. The CV% of negative signal and standard deviation were 21.6±23.6 (mean ± S.D.). MFIs of hybridization signals were clearly high only when the oligoprobes matched the mutations in the fragments (Fig. 2B). These data confirmed that the assay system could discriminate one base mismatch at M41, K65, K70, K103, M184 and T215 codons in the plasmid-probe model system.

Next, we examined the sensitivity to detect a particular sequence in a mixture for each DR-related site. The plasmids carrying the wild type and mutant sequences were mixed at various ratios. In samples containing only the wild type sequences, the mean background signal (% ±2SD) was 2.0% ±1.2, 4.1%

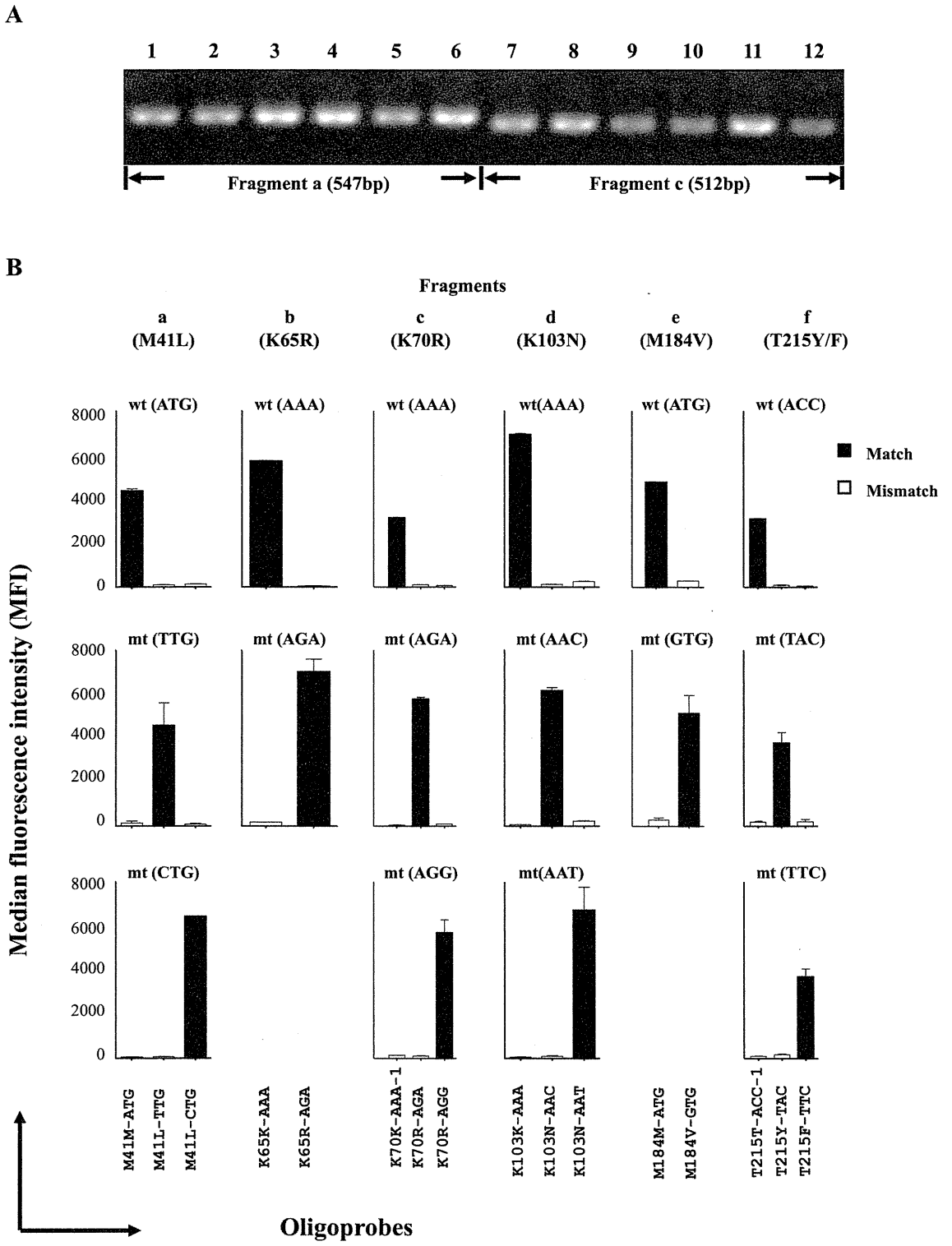

Figure 2. Validation of PCR-SSOP-Luminex assay using plasmids as templates. (A) Agarose gel electrophoresis of amplified fragments. Lanes 1–6: Fragment a (547 bp). Lanes 7–14: Fragment c (512 bp). 1, wild type; 2, M41L-TTG; 3, M41L-CTG; 4, K65R-AGA; 5, 70R-AGA; 6, 70R-AGG; 7, wild type; 8, 103N-AAC; 9, K103N-AAT; 10, M184V-GTG; 11, T215Y-TAC; 12, T215F-TTC. (B) Median fluorescence intensities (MFIs). The plasmid in the test sample is indicated on the top of each panel. Oligoprobes used for detection are indicated at the bottom. Matched results are shown as black bars, mismatched results as white bars. Assays were performed in triplicate. The mean ± standard deviation is shown at the top of each bar.
doi:10.1371/journal.pone.0109823.g002

±2.6, 3.3% ±1.2, 4.6% ±1.8, 6.2% ±3.2 and 3.3% ±0.4 at M41, K65, K70, K103, M184 and T215, respectively (Fig. 3B). The signal for the mutant was judged positive when "% signal" from the mutant oligobeads exceeded the mean + 2SD; 3.2%,